

FILM COOLING FROM CYLINDRICAL HOLES IN TRANSVERSE SLOTS

A Thesis

**Submitted to the Graduate Faculty of the
Louisiana State University and
Agricultural and Mechanical College
in partial fulfillment of the
requirements for the degree of
Master of Science in Mechanical Engineering**

in

The Department of Mechanical Engineering

by

Mohammed S. Altorairi

B.S., King Fahad University of Petroleum and Minerals (KFUPM), 1996

August 2003

Acknowledgements

For every work there is a key for success. The key of success for this study was the great support I received from my advisor Dr. Srinath V. Ekkad. He did not spare any effort to make the experiment possible and meaningful. He shared with me his previous experience and work on this field. I was always provided easy access to all necessary resources and technical references. For his patience and great attitude, this work progressed smoothly regardless of the unexpected obstacles we faced. Dr. Ekkad was always available for technical consolation, which reflected positively on this study. His initial guidance and continues directions were my foundation.

I will also like to thank Dr. Yitshak Ram and Dr. Ramachandra Devireddy for participating in my MS committee as members. I would like to thank my lab colleague Hasan Nasir for his valuable suggestions and contributions during experimental study. Many thanks go to Ryan Hebert for their support and help. I would also like to thank Gautam Pamula for developing the macro used in this study. Special thanks go to my lab colleague Vikrant Saxena for his help and support.

Table of Contents

Acknowledgement	ii
List of Figures	v
Nomenclature	viii
Abstract	ix
Chapter 1. Introduction	1
1.1 Turbine Blade Cooling, an Engineered Solution	1
1.2 Film Cooling	2
1.2 Literature Survey	5
1.3 Objective of the Present Study	10
Chapter 2. Experimental Set-Up	11
2.1 Blower	11
2.2 Heater	12
2.3 Baffles and Mainstream Inlet	13
2.4 Coolant Section	14
2.5 Test Section	15
2.6 Hole Geometry	16
Chapter 3. Measurement Tools	19
3.1 Temperature Acquisition System	19
3.2 Visual Image Processing System	20
3.3 High Pressure Compressor	23
Chapter 4. Theory and Data Reduction	24
4.1 Heat Transfer Theory	24
4.2 Data Reduction	28
Chapter 5. Results: Heat Transfer Measurements	31
5.1 Baseline Case	31
5.1.2 Span Averaged Heat Transfer Coefficient	31
5.1.3 Span Averaged Adiabatic Film Effectiveness	34
5.2 Slot Case	38
5.3 Double Shoulder Case	42
5.4 Right Shoulder Case	46
5.5 Angled Case	50
5.6 Summary of Cases	54

Chapter 6. Conclusions	56
6.1 Recommendation for Future Work	57
References	58
Vita	60

List of Figures

Figure 1.1	Typical film cooled turbine blade.....	1
Figure 1.2	Protective film layer made by coolant injection	2
Figure 1.3	Various types of blade air cooling	4
Figure 1.4	The direction convention for streamwise and spanwise in a typical case of compound angle	8
Figure 2.1	General layout of the experiment component	11
Figure 2.2	The variable speed blower	12
Figure 2.3	Side view of the wind tunnel	13
Figure 2.4	The by-pass gate	13
Figure 2.5	The temperature control of coolant flow	14
Figure 2.6	Flow mixing in test section	15
Figure 2.7	The test plate dimensions	16
Figure 2.8	Case 1 (normal)	16
Figure 2.9	Case 2 (slot)	17
Figure 2.10	Case 3 (right shoulder)	17
Figure 2.11	(double shoulder).....	18
Figure 2.12	Case 5 (angled)	18
Figure 3.1	Instrunet interface terminal box	19
Figure 3.2	The PC to Instrunet interface	20
Figure 3.3	Plunix camera	20
Figure 3.4	RGB camera setup	21
Figure 2.2	The high pressure compressor	23
Figure 4.1	Typical convective heat transfer problem	24
Figure 4.2	Coolant injection problem	26

Figure 4.3	First transient test used to compute h and η	28
Figure 5.1	Baseline h for $M= 0.5$ & 1.0	31
Figure 5.2	Local heat transfer coefficient for $M= 0.5$ & 1.0	33
Figure 5.3	Baseline η for $M= 0.5$ & 1.0	35
Figure 5.4	Local film effectiveness for $M= 0.5$ & 1.0	37
Figure 5.5	Average h for slot case	39
Figure 5.6	Normalized average h for slot case	39
Figure 5.7	Averaged η for Slot case	39
Figure 5.8	Normalized η for Slot case	39
Figure 5.9	Local heat transfer coefficient for $M= 0.5$ & 1.0 for slot case	40
Figure 5.10	Local film effectiveness for $M= 0.5$ & 1.0 for slot case	40
Figure 5.11	Average h for double shoulder case	44
Figure 5.12	Normalized average h for double shoulder Case.....	44
Figure 5.13	Averaged η for double shoulder case	44
Figure 5.14	Normalized η for double shoulder case	44
Figure 5.15	Local heat transfer coefficient for $M= 0.5$ & 1.0 for double shoulder case	45
Figure 5.16	Local film effectiveness for $M= 0.5$ & 1.0 double shoulder case.....	45
Figure 5.17	Average h for right shoulder case	48
Figure 5.18	Normalized average h for right shoulder case.....	48
Figure 5.19	Averaged η for right shoulder case	48
Figure 5.20	Normalized η for right shoulder case	48
Figure 5.21	Local heat transfer coefficient for $M= 0.5$ & 1.0 for right shoulder case	49
Figure 5.22	Local film effectiveness for $M= 0.5$ & 1.0 for right shoulder case	49
Figure 5.23	Average h for angled case	52

Figure 5.24	Normalized average h for angled case	52
Figure 5.25	Averaged η for angled case	52
Figure 5.26	Normalized η for angled case	52
Figure 5.27	Local heat transfer coefficient for $M= 0.5$ & 1.0 for angled case	53
Figure 5.28	Local film effectiveness for $M= 0.5$ & 1.0 for angled case	53
Figure 5.29	The total normalized heat transfer coefficient for all cases	54
Figure 5.30	The total η/η_0 for all cases	55

Nomenclature

d	hole diameter
h	convective heat transfer coefficient
k	thermal conductivity of Plexiglas test surface
M	blowing ratio
p	slot depth
P_c	coolant flow pressure
P_m	mainstream flow pressure
q''	heat flux
S	slot width
t	time of color change
T_c	coolant temperature
T_f	film temperature
T_i	initial temperature of the test plate
U	flow velocity
X	streamwise distance
a	thermal diffusivity of test surface
η	adiabatic film effectiveness, $\frac{T_f - T_m}{T_c - T_m}$
μ	fluid dynamic viscosity
ρ	fluid density

Abstract

In this study, heat transfer coefficient and film effectiveness distributions are investigated for a film cooling hole configuration that has inclined holes discharging into a tangential slot before interactions with the mainstream. The cylindrical holes are inclined 35° along the mainstream direction. The effect of coolant-to-mainstream blowing ratio is examined for $M=0.5$ and $M=1.0$. Different slot width to hole ratios and also the effect of hole exit condition (square edge and triangular edge) is considered. The mainstream velocity and free-stream turbulence intensity in the low speed wind tunnel are 9 m/s and 7% respectively and the mainstream Reynolds number based on hole diameter is around 7,100. The intent is to come up with an optimum hole exit geometry associated with low convective heat transfer coefficient h . Also the adiabatic film effectiveness h should be as high as possible. For this purpose, different whole exit geometries were tested for an optimum shape. Heat transfer calculations were made to obtain the local values for h and h . The first case tested were the “normal” 35° with 0.5 inch diameter inclined hole. The second was the “slot” with height to hole diameter ratio (p/d) is 0.4 and width to hole diameter ratio (W/d) = 1.75. The third was the right shoulder with (W/d) = 1.375. The fourth and fifth cases are the “double shoulder” with (W/d)= 1.0 and the “angled” with a varying ratio (W/d). The angled is featured with 18° inclined right attachment. The results of all cases were referenced to the normal case as a baseline. The right shoulder case presented the best performance with a uniform jet scattering. The right shoulder geometry is more likely to protect and cool the blade than the normal geometry, as its total adiabatic film effectiveness was better than baseline case

with factor of 1.4 and the total heat transfer coefficient was less than baseline case with factor of 0.08. This means it will exchange less heat and provide a better film.

Chapter 1

Introduction

1.1 Turbine Blade Cooling, an Engineered Solution

Over the past fifty years, aircraft and power generation gas turbine designers have endeavored to increase the combustor exit and high-pressure turbine stage inlet temperatures. With higher combustor exit temperatures, improved efficiency and reduced fuel consumption can be achieved. Similarly, in aircraft application, the higher temperatures lead to increased thrust. Unfortunately, these higher temperatures have a negative effect on the integrity of the high-pressure turbine components and specifically the turbine blades. Therefore, there is a need for an efficient cooling system engineered in a way such that the maximum blade surface temperature during operation is not more than the maximum melting point of the blade material.

To achieve that, researchers focus on various innovative cooling techniques. Depending on the nature of the coolant flow, the cooling methods currently implemented in the turbine industry can be classified into two types: internal cooling and external cooling. In the first type cooler air is bled from the compressor stage and then passed through internal passages incorporated into blade designs for this purpose. This is the most

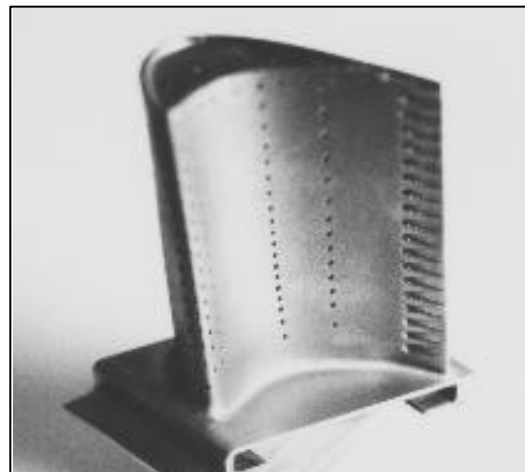


Figure 1.1 typical film cooled turbine blade (*Heat Transfer Laboratory, University of Minnesota*)

common technique and is called enhanced passage cooling. For maximum heat absorption, the air is also allowed to impinge on the internal wall of the blade. This technique is called impingement cooling. In external cooling, air is bled from the compressor stage, ducted through the internal chambers of the turbine blades, and then discharged through small holes/ slots on the blade outer walls. This air provides a thin, cooler, insulating film along the external surface of the turbine blade, due to which the method is called “film cooling.” That film provides protection and thus increases the life of the blade. This life maybe reduced by 50% if the blade’s operating temperature was off the maximum design temperature by 50°F.

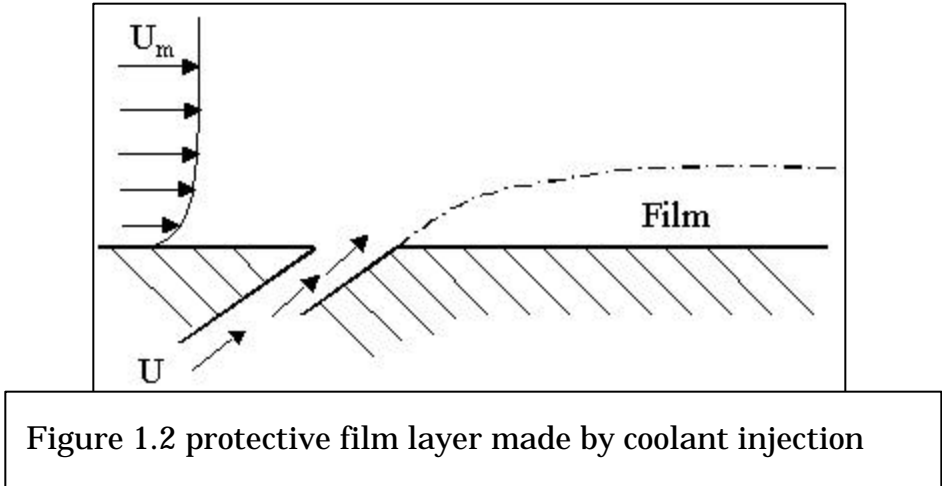


Figure 1.2 protective film layer made by coolant injection

1.2 Film Cooling

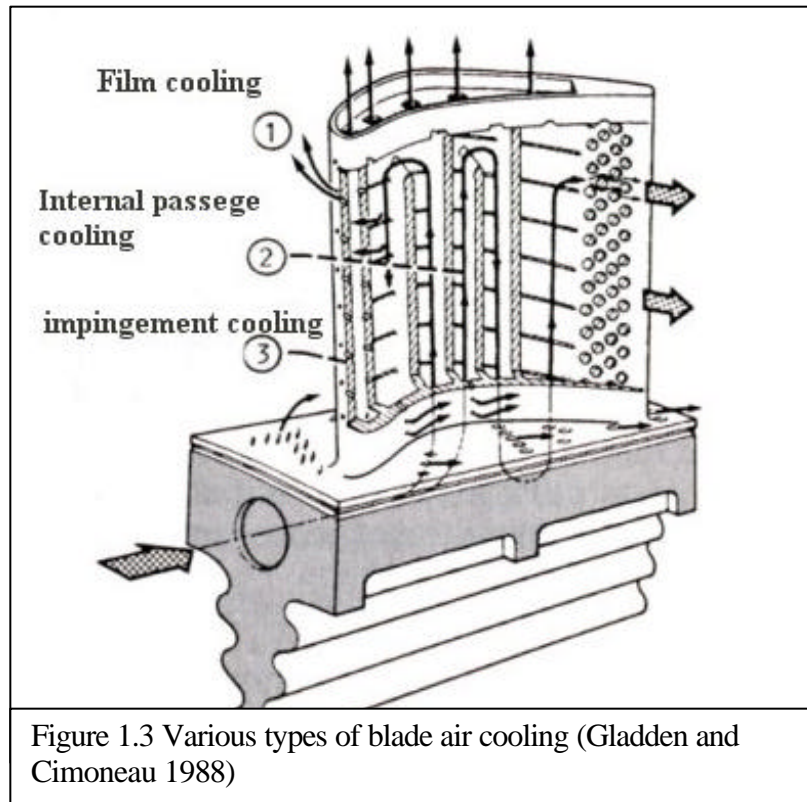
To better understand film cooling, let’s consider a simple case where mainstream and air coolant are mixed up as shown in figure 1.2. If there was no coolant, no film, then the heat transfer will be of a simple convection mode and the rate of heat transfer per unit area is $q'' = h(T_m - T_w)$, where h is local heat transfer coefficient and $(T_m - T_w)$ is the local temperature difference between the surface of the blade and mainstream. Heat flux

(q) represent the heat exchanged between the hot air and turbine blade. It should be obvious that keeping this value to a minimum is desirable. For this purpose, the film introduced creates a protection zone between the hot air and surface of the blade.

The success of designing a good cooling technique with a effective film is measured mainly by two parameters. The first parameter is the local heat transfer coefficient (h). As discussed above it is desirable to keep (h) as low as possible. The second factor is film effectiveness (η). Both the film effectiveness (η) and (h) will be discussed in depth in Chapter 4. However it is imperative, for now, to introduce the film effectiveness as an indication of the film effectiveness of the protective film. This effectiveness is simply temperature difference ratio of film-mainstream to film-coolant. Thus the mathematical representation is $\eta = \frac{T_f - T_m}{T_c - T_m}$, where $\eta = 1$ represents perfect film and $\eta = 0.0$ represents no film.

According to Han et al. (1999), there are other factors researchers consider when investigating a possible design. The first factor is the coolant-to-mainstream pressure ratio (P_c/P_m). This ratio could be related to the coolant-to-mainstream mass flux ratio or what is known as the blowing ratio. In typical gas turbine airfoil, the (P_c/P_m) ratio ranges from 1.02 to 1.1 while the corresponding blowing ratio is within 0.5 to 2.0. The second factor to be considered is the coolant-to-mainstream temperature ratio (T_c/T_m). This ratio is related to the density of each flow and its values ranges from 0.85 to 0.5. While fixing the temperature ratio, increasing pressure ratio results in lower heat transfer to airfoil and hence better film protection. When switching parameters, the opposite logic applies and film protection decreases if we fix the pressure ratio while keeping the temperature ratio

high. Yet these trends should be treated as general indications as the optimum value will vary for each case.



In an attempt to produce better film cooling design, researchers have performed extensive heat transfer analysis studying the effect of changing any of the parameters discussed above. To facilitate producing detailed quantitative data from experimental tests, a new technique called “transient liquid crystal technique” was employed by some researchers. This technique provides visual temperature sensing at areas coated with thermo-chromic liquid crystals. With the aid of an appropriate digital image capturing system, one can record the temperature profile with respect to time at each point of the blade surface. The liquid crystals are factory calibrated at a specific temperature to change color at a certified temperature. Ekkad (1995) published a comprehensive report

for his PhD thesis in which he elaborated extensively on the liquid crystal technology. This report provide an excellent reference for technical information regarding the implementation of this technology in studying film cooling.

It is always desirable to keep the blades in the lowest possible range of operating temperature, however, there is a hefty price for supplying too much cooling flow. Since the coolant air is supplied from the compressor stage, only 8-9% of the total air exiting the compressor could be bled. This could be understood knowing the mass flow rate air exiting the compressor affects the compressor efficiency and hence the overall performance of the turbine engine. Keeping this last fact in mind, researchers had to work with the available coolant flow rate and investigate possible methods to better handle the coolant air such that the film produced provide the maximum protection or effectiveness. This was basically the motivation behind all studies on this field with the challenge of a limited coolant flow. For this purpose researchers studied each aspect that could contribute to better film effectiveness and lower heat transfer coefficient. Following is a survey of the work done on this field for a flat surface.

1.3 Literature Survey

The first use of liquid crystal was by Cooper et al. (1975) and Simonich and Moffat (1984). Although the resolution of their measurement was not high, they were able to successfully study convective heat transfer and obtain local heat transfer coefficient of a plain plat. Through out their work, they had to rely on visual detection to track the color change of their test section. Camci et al. (1992) presented a hue-capturing technique to analyze the liquid crystal images. With the use of 24-bit color images, their technique could apply to both steady and transient heat transfer measurement. With the exception

of few, all researchers conducted their tests on a flat surface. This due to the fact it is extremely difficult to run a film cooling experiment under real engine condition. Among to first to examine film-cooling in their research were Goldstein and Taylor (1982). Their first results suggested that heat transfer coefficient downstream of film injection was enhanced because of the turbulence produced by mixing coolant jet with mainstream boundary layer. In their study, the holes were a simple 35° inclined along the mainstream flow direction. They also found that, at a lower blowing ratio ($M < 0.8$), the coolant jet could not divert the forward movement of the mainstream at mixing point or at the hole. Only at large blowing ratio, the coolant jet was able to push mainstream back and jet formed a solid protective layer in the shape of a rod. Before that, Goldstein et al. (1972) conducted a pioneer study, involving the effect of diverging and elliptical hole exits with 35° angle. The holes were 3-D apart and while the diverging angle was 10° in one case. Their study was backed up by flow visualization that explained the flow behavior before and after mixing. Results showed appreciable increase in centerline film effectiveness for diverging case over the elliptical one. This was due to the decrease in velocity of the secondary flow with the diverging exit shape. This, accordingly, caused the jet to stay closer to surface of the wall rather than penetrating into the mainstream. The increase in film effectiveness was independent of the blowing ratio for small X/d , where X/d is the distance downstream the hole.

Makki and Jakubowski (1986) conducted an experimental study testing the effect of trapezoidal shaped holes on local heat transfer coefficient (h). They were able to prove an improvement of 23% in film effectiveness for the test shape over the circular one. They

predicted the improvement was attributed to the enhancement in the turbulence in three regions:

- (i) The mixing process along the mainstream cross flow.
- (ii) The penetration of the mainstream flow between the coolant jets downstream the holes.
- (iii) The mixing process within the coolant jet itself with formation of the counter-rotating vortices.

Taslim et al. (1990) examined the effect of slot exit geometry on film effectiveness (η) for several injection angles. Limiting his case to the trailing edge area with a fixed blowing ratio ($M=1.4$), Taslim concluded that the optimum angle is 8° . In their study for a leading edge case, Karni and Goldstein (1990) looked at the effect of injecting from cylindrical holes utilizing the mass transfer technique. With injection angles ranging from 10° to 37° , the increase in the blowing ratio was observed to enhance the film effectiveness. Ligrani et al (1994) presented heat transfer coefficient for a row of compound angle holes with six diameter spacing. They compared simple angle holes with compound angle holes. Confirming with previous studies, film effectiveness was better with the compound angle. Sen et al. (1996) conducted a study similar to Ligrani experiment with the addition of forward 15° expanding (streamwise) hole and 60° in the spanwise direction. For almost all blowing ratios, the last case showed the worst performance in terms of heat transfer coefficient.

Schmidt et al. (1996) presented local and span-averaged adiabatic film cooling effectiveness (η) distribution measured downstream of three different geometries: (i) round, (ii) round compound angle, and (iii) forward diffused, compound angle. The two

compound angles arrangements gave higher effectiveness (η) over larger range of momentum flux ratio than the simple angles arrangement. Differences in effectiveness magnitude were apparent at high momentum flux ratio and $X/d < 15$.

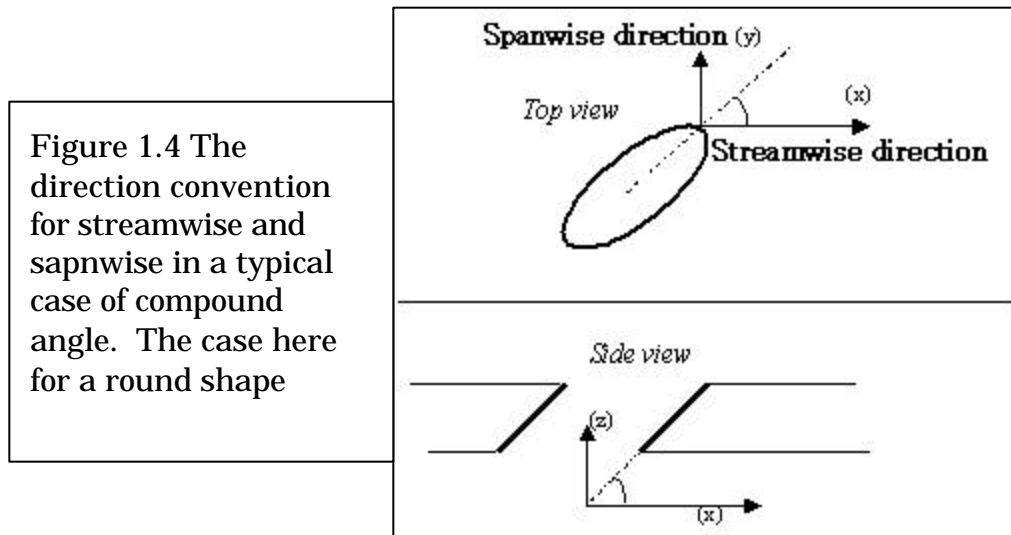


Figure 1.4 The direction convention for streamwise and spanwise in a typical case of compound angle. The case here for a round shape

Ekkad et al. (1997a,b) compared two compound-angle holes with simple angle injection. All holes were inclined 35° streamwise. The compound angles were 45° and 90° in the spanwise direction. Compound angle injection provided higher heat-transfer coefficient than simple holes. Simple injection causes limited interaction between mainstream and coolant jets. The jet structures move spanwise along the hole and dissipate at slower rate compared to that for compound-angle injection. They also showed that compound angles provide significantly higher effectiveness over a large area than the simple angle case.

Grtisch et al. (1997) investigated three different shapes: (i) round, (ii) latterly diffused, and forward-latterly diffused. The uniqueness of Grtisch's experiment was to use a high-speed flow. The film effectiveness (η) span-averaged values of expanded exit

case were significantly higher than others. At the same time, the heat transfer coefficient was high for round shape holes. The reason for getting lower (h) for expanded holes is the spread out of the jets laterally. Chen et al. (1998) tested a new type of expanded holes using conical holes, with different compound angle orientations. The best over all performance was obtained from conical holes with 0° compound angle. As expected, the worst case was with conical holes and 90° compound angle. It was understood the 90° angle caused a penetration of the jet into the mainstream preventing the formation of an effective film.

Bunker et al. (2002) tested hole-within-slot cases. The two tested cases were: radial rounded and radial in slot. The slot was fed by a row of discrete coolant supply holes oriented in the spanwise direction with inclination angle of 30° . The slot depth to hole diameter ratio (P/d) was 4 and 0.43. The last case is called shallow trench. Bunker investigated the effect of the slot width also for width to diameter ratio (W/d) of 1.16, 1.5 and 2.0. Bunker concluded that the best performance is found with the narrowest slot. He also predicted an improvement of 50-75% in the film effectiveness for the shallow trench case for $X/d < 40$ compared to trench-less injection.

Several aspects of film cooling have been investigated in the past. The potential of predicting indicative values of the heat transfer coefficient and film effectiveness for slot-in-hole and angled slot was the motivation for this study based on the sample results presented by Bunker et al. The present study is investigating several hole-in-slot cases with varying slot width and shape. The cases are:

- (i) Normal case with 35° angle in the spanwise direction.

- (ii) Slot case in the 0.5 inch hole is centered in a 1.75 inch slot with (p/d) of 0.4 and (W/d) of 1.75.
- (iii) Right shoulder case in which the same slot case is modified with right fixture making the (W/d) equals to 1.375 and hole becomes uncentered inside the slot.
- (iv) Double shoulder case in which the slot case is modified with two identical fixtures making (W/d) of 1.0 and hole becomes centered.
- (v) The angled case is case (ii) with slanted right fixture with an angle of 18° .

All cases are investigated with the transient liquid crystal technique.

1.4 Objective of the Present Study

The objectives of the present study are:

1. To study the effect of different hole geometries on film effectiveness (η)
2. To study the effect of different hole geometries on local heat transfer coefficient (h)

Both objectives are investigated for two blowing ratios, $M=0.5$ & 1.0 .

Chapter 2

Experimental Set-Up

All experiments were carried out in a low-speed wind tunnel setup with compressed air supply for coolant air. Figure 2.1 shows a general layout of the experimental arrangement. The test setup consists of:

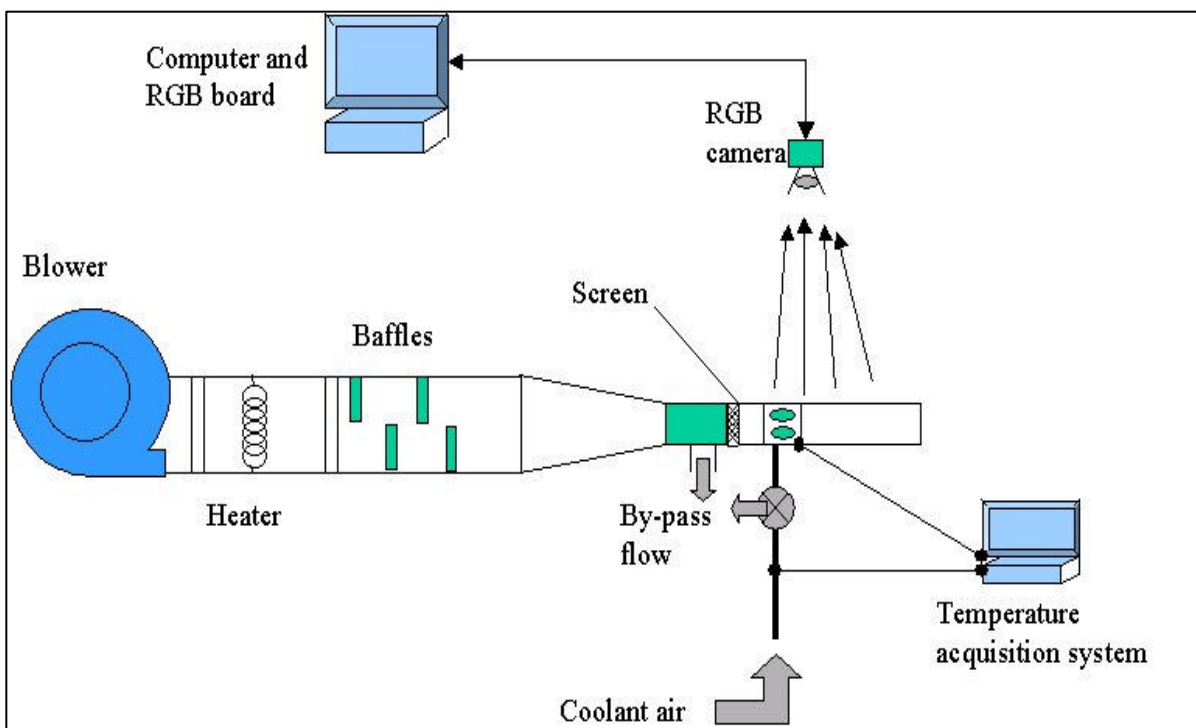


Figure2.1 General layout of the experiment components

2.1 Blower

A variable speed blower that can deliver up to 12 m/sec mean velocity inside the tested section. The blower is driven by $\frac{1}{2}$ horsepower motor with 1725 rpm as a maximum

speed. As shown in figure 2.2, the blower speed is controlled by variable DC source. The purpose of the blower is to provide the mainstream flow.



Figure2.2 the variable speed blower

2.1 Heater

The blower is connected to a 12 kW heater that heats up the air to a free-stream temperature of 58-60°C. The heater is composed of multiple high voltage resistances capable of reaching a steady state temperature for 9 m/sec flow in less than 12 minutes. The temperature at the Turbine Heat Transfer Lab was not constant through out all the tests. For that, it was hard to maintain the flow temperature at the same range for all tests. This problem was overcome by preheating the air-feed to the blower, as needed, with either a 1500 W or a 3000 W heater. The temperature of the flow downstream of the

heater is continuously monitored by a thermocouple connected to the temperature acquisition system (see chapter 3).

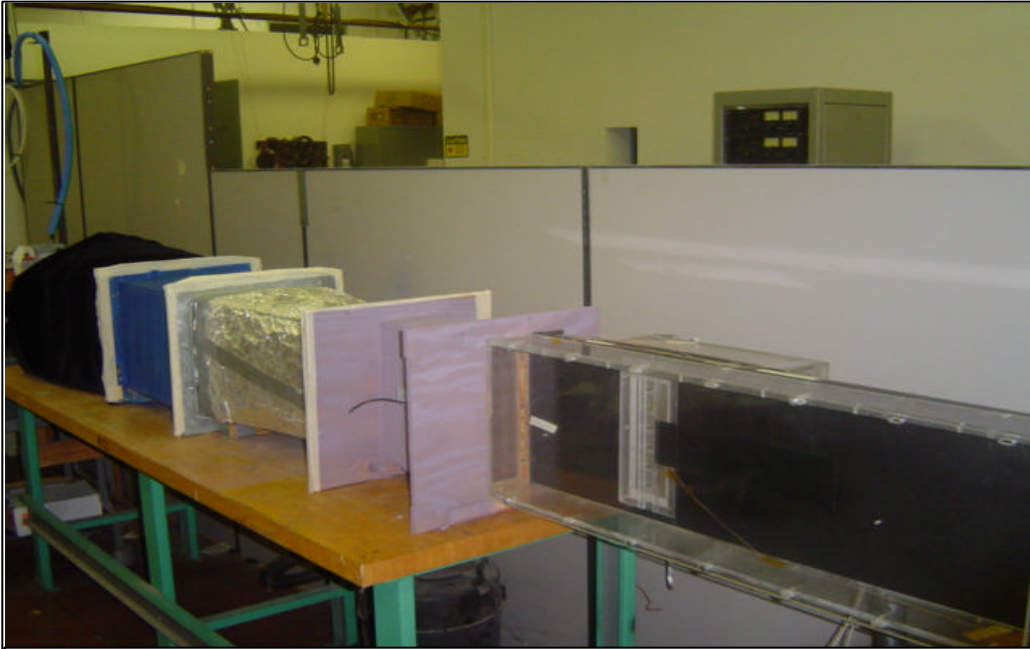


Figure 2.3 Side view of the wind tunnel

2.3 Baffles and Mainstream Inlet

In this section the air is routed through a section with baffles then passes through a 4:1 2-D converging nozzle. This ensures adequate mixing of hot air and uniform temperature distribution throughout the test section. It is true that this experiment uses the transient liquid crystal technique yet the flow from both the coolant and the mainstream



Figure 2.4 The by-pass gate

must to be at steady state prior to mixing. This ensures that $dT/dt=0$ @ $X= -X/d$ and $t=0$ where t is time, $-X/d$ is the any short distance before the test section. For this purpose, a by-pass gate (figure 2.4) was

installed just before the inlet of the mainstream. Thus, the mainstream air exiting the nozzle is initially routed out away from the test section through the open by-pass gate to the outside space. This allows the main flow to reach the desired steady state temperature. When that temperature is reached, the gate is closed forcing the flow into the test section.

2.4 Coolant Section

The coolant air is provided by a 290 psi compressor. Through a manual control valve (MCV), the coolant flow is adjusted to the desired value that satisfy the mass flux ratio M , where M is defined as follows:

$$M = \frac{(rU)_c}{(rU)_m}$$

Where $(rU)_c$ is the mass flux of the coolant and $(rU)_m$ is that mean stream. The coolant flow passes through a pipe heater. The heater is voltage-controlled and can provide up to 90° C flow temperature for $M=1.5$. The purpose of the heater is to maintain the coolant flow within the desired range for each case. As it was the case for the mainstream, the coolant needs to have a steady state temperature just before mixing. For this purpose a three-way valve was installed. The valve diverts the cooler air away from the test section till its temperature is stable enough. The valve is then flipped open directing the flow into the test section. This should to be synchronized with the closing of the by-pass gate on the mainstream.



Figure 2.5 The temperature control of coolant flow

2.5 Test Section

Finally the flow from the coolant holes and the mainstream combine in the test section as shown in the Fig 2.6. The test section is made of Plexiglas[®] and has a cross-section of 30-cm width and 9-cm height. The components upstream of the test section are covered with insulation to minimize the heating time. The bottom plate of the test section

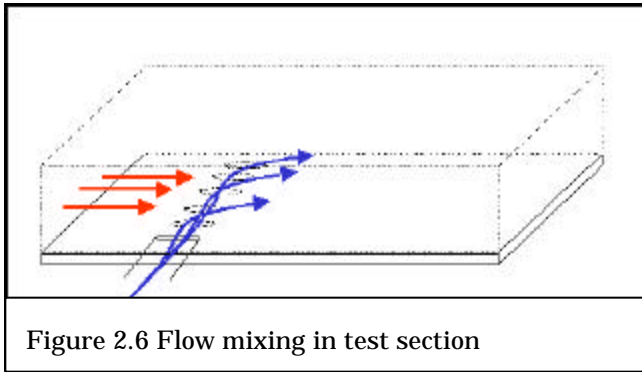


Figure 2.6 Flow mixing in test section

is made of 2.22-cm thick Plexiglas.

This plate has a replaceable section about 25.4 cm downstream of the test section inlet (see figure 2.7).

This replaceable section can be

interchanged to accommodate the hole geometry. A trip is placed at the entrance to the test section to produce a fully turbulent boundary layer over the test plate. The film holes are located 30.5 cm downstream of the trip. The coolant air is provided from a separate compressed air supply and is metered for flow measurement. Thermocouples are mounted upstream of the hole row to measure the mainstream temperature, and inside one of the holes to measure the coolant exit temperature.

Figure 2.7 shows the test plate with film hole geometry used in this study. There are six holes of 0.5-inch diameter in each row. The spacing between adjacent holes is 3 hole diameters for all the hole. Since the flow is assumed to be equally distributed through all holes, only the middle two holes are considered during testing. The flow is even in the middle holes. This also to reduce the measurement area and save time in computation.

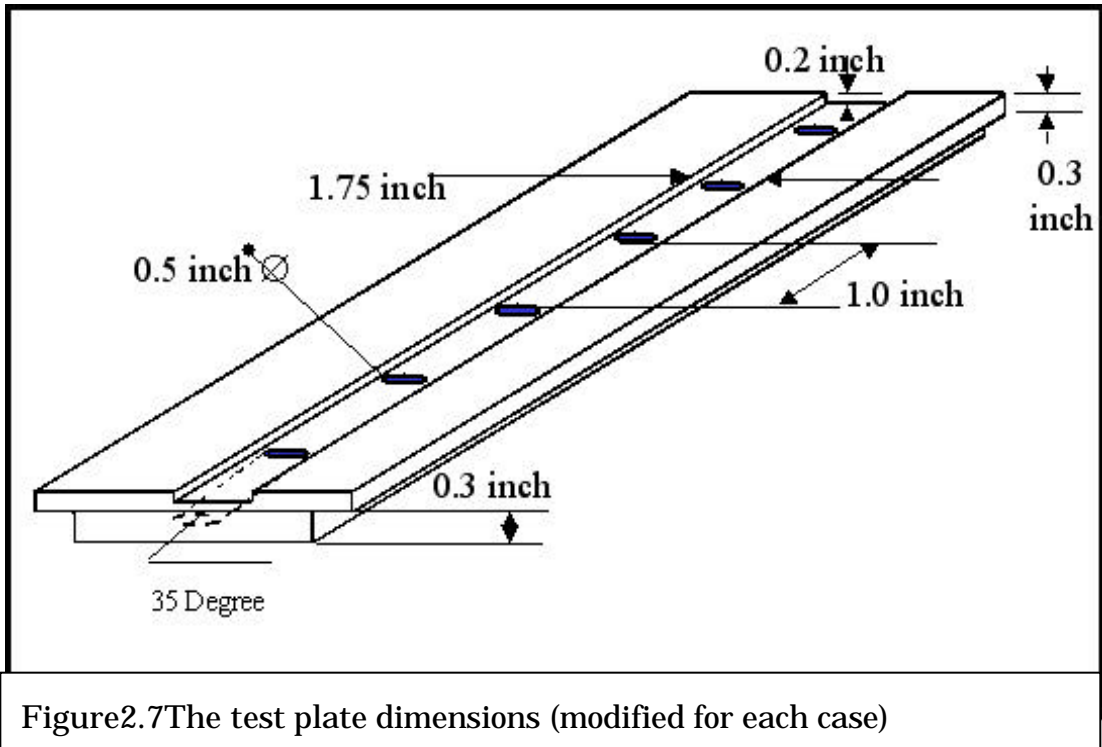


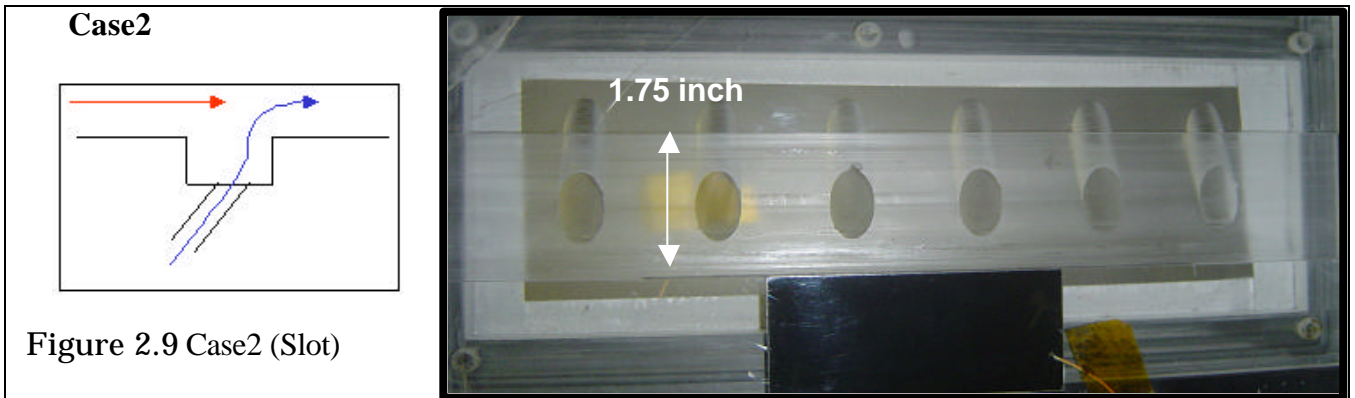
Figure 2.7 The test plate dimensions (modified for each case)

To accommodate the geometry of each case the retractable part of the test section, as shown in figure 2.7 and 2.8, is modified. This part is also made of Plexiglas[®] and has been supplied with several attachments and fixtures. These attachments provide the desired hole geometries discussed in the next section.

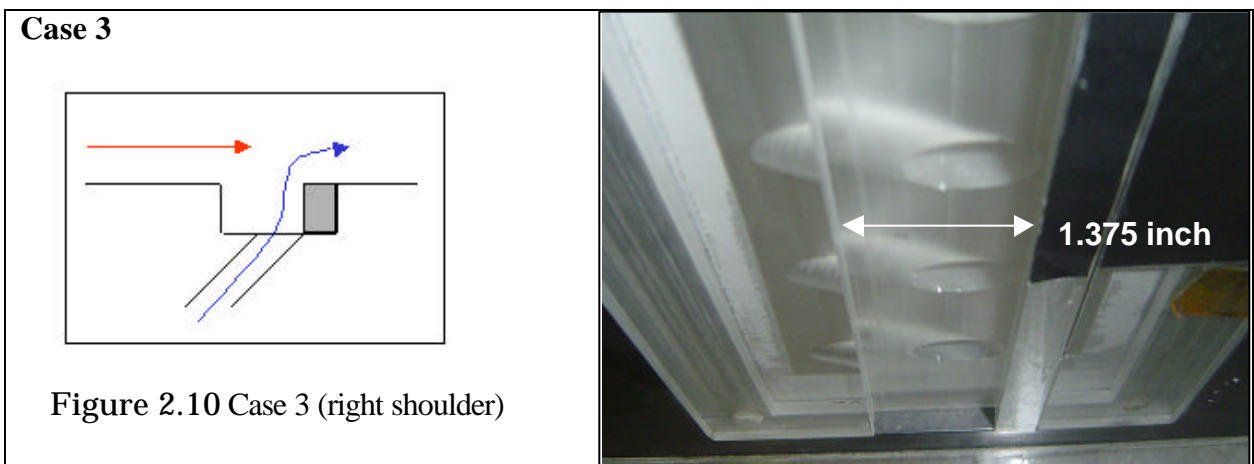
2.6 Hole Geometries



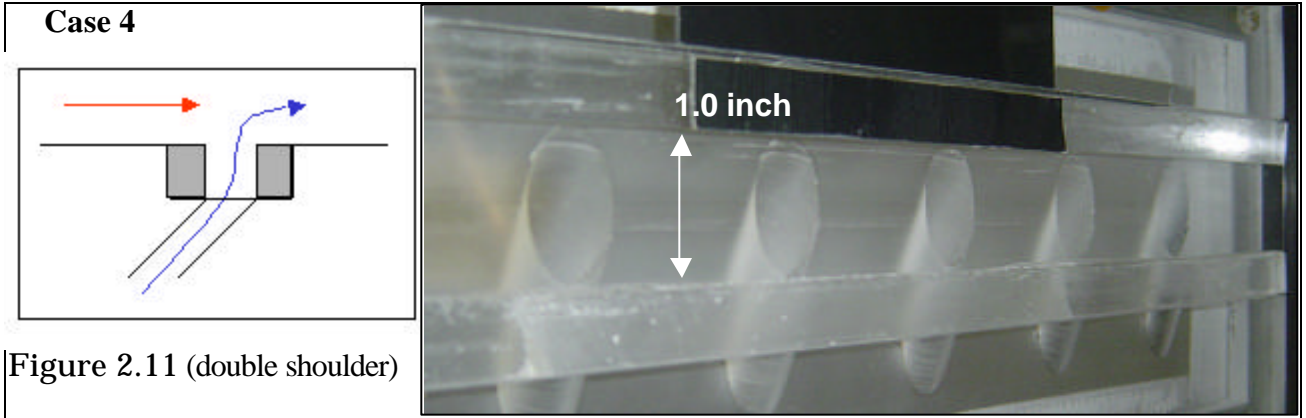
In this case, the coolant flow mixes up with the mainstream directly at a 35° angle.



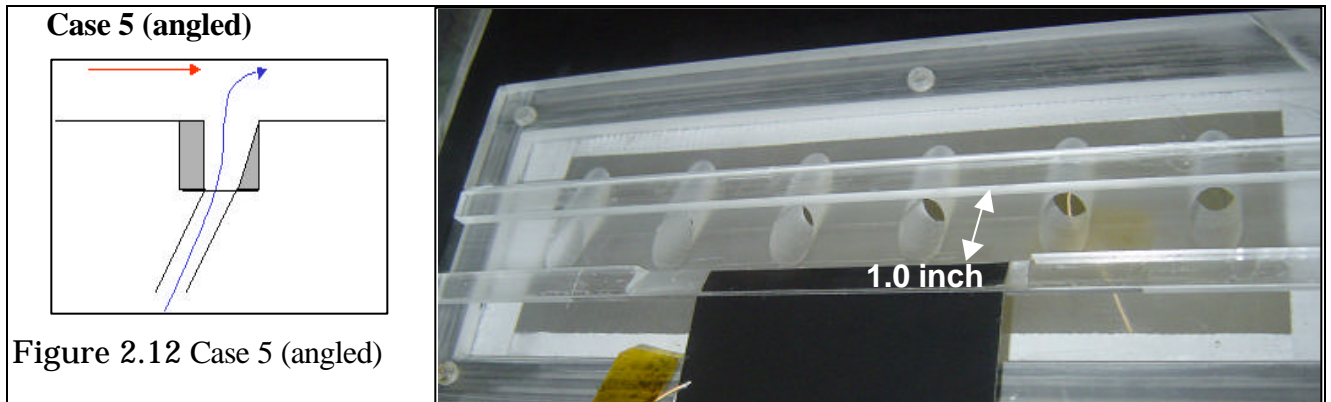
The hole in this case is positioned inside a 1.75in wide and 0.2 in height slot. Thus, the height to hole diameter ratio (p/d) is 0.4. The slot width to hole diameter ratio (W/d) = 1.75.



This case is similar to case two except the width of the slot is 1.125in. The p/d ratio is still 0.4. The slot width to hole diameter ratio (W/d) = 1.375.



The flow in this case goes from 35° to 90° then merges with the mainstream. The slot width to hole diameter ratio (W/d) = 1.0.



The right side of the slot in this case is slanted with 18° slop. The p/d ratio is 0.4. The slot width to hole diameter ratio (W/d) = 1.0.

Chapter 3

Measurement Tools

3.1 Temperature Acquisition System

During each run of the experiment, the temperature of five points at the test section are monitored and recorded. The points at which the temperature is collected are:

- (i) The mainstream before the test section. This is to ensure the steady state temperature is reached before closing the gate.
- (ii) The mainstream temperature in the test section.
- (iii) The surface temperature near the hole.
- (iv) The coolant temperature before the test section. This is to ensure the steady state temperature is reached before flipping the three-way valve.
- (v) The coolant temperature just before it emerges into the mainstream.

Figure 3.1 Instrunet interface terminal box



The temperature is sensed using K type thermocouples. The thermocouples are linked to a PC with *InstruNet* interface. *InstruNet* is a data acquisition hardware that provides microVolt inputs/ outputs of high accuracy. The external box, (see figure 3.1), contains signal conditioning amplifiers for each channel, and can therefore directly attach to sensors such as thermocouples, RTD's, strain gauges, resistance sources, current sources, and voltage sources; and return engineering units (e.g. "Volts","Amps"). *InstruNet* provides 14-bit resolution in the micro-volt range, with analog inputs with +/-5V, +/-6V, +/-0.08V & +/-0.01V range for 44 terminals. The controller's themselves provide 10 counter/timer channels that each can function as a digital input bit, a digital output bit, a clockoutput channel, or a period measurement input channel.

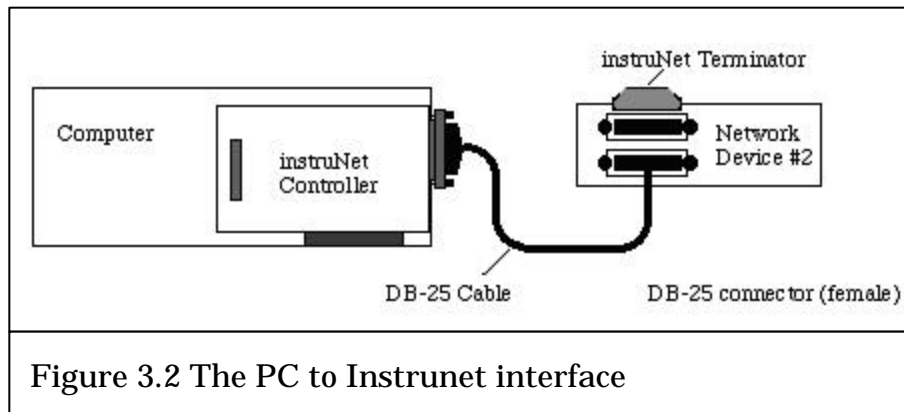


Figure 3.2 The PC to InstruNet interface

3.2 Visual Image Processing System

A schematic layout of the image processing system used for this test facility is shown in the Figure 3.4. A Plunix RGB camera is placed 12 feet away from the test section. Although the test section is enclosed



Figure 3.3 Plunix camera

within a rectangular wind tunnel (see figure 2.6), the transparent plexi-glass allows the camera to capture “time” frames accurately. This camera connects to a CFG 24-bit frame grabber board in a PC.

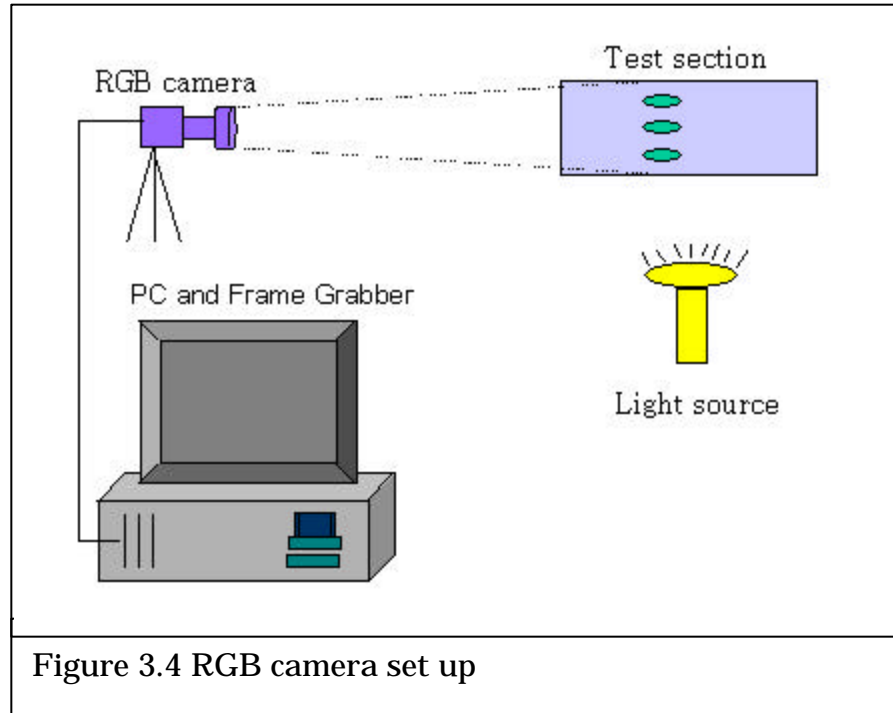


Image processing software (Optimas v6.5) communicates with the frame grabber board. The camera records the local RGB value on the test section. Using a customized macro, Optimas tracks the green band in each pixel. This macro works by simply recording the time at which green color appears on each pixel. For this to work effectively, the background intensity of the test section must be set properly. The maximum background intensity is called “threshold.” The appropriate setting of the threshold is important as it determines the criteria for the color change captured in each frame. If the local pixel intensity exceeds the threshold value then Optimas acknowledges color change and records a time value for that pixel. To enhance the time values file, adequate

lighting is evenly provided for the test section. The appearance of many zeros in the time file could be attributed to the following:

- (i) Insufficient or improper lighting distribution as the light intensity should be even on all areas of the test section.
- (ii) Low threshold value or wide threshold profile. The threshold profile must be as narrow as possible. A wide profile indicates uneven lighting.
- (iii) Low contrast and brightness value. Through Optimas control option, these value can be adjusted prior to the start of each macro.
- (iv) Bad liquid crystal sheet. If the crystal sheet are over used or exposed to light for a long time, then it may not change color as calibrated.
- (v) Very hot flow. If the both the coolant and the mainstream are at very high temperature (above 65C), then the camera might not capture the green band on X/d less than 5. Although the camera is designed to capture 4-5 frames per second, actual runs have proven that the transition time for green band could take less 0.25 sec.

Another important aspect to pay attention to is the capture area within the test section. The area selected is defined in terms of X, Y, and size in pixel. These three parameters must be kept constant for each pair of runs (hot and cold). This is essential, as each pair will be used to calculate the heat transfer coefficient and film effectiveness for a single area. Keeping the size constant is easy and could be done through Optimas. However, the X and Y coordinate needs special attention as the camera should not be moved or touched between runs.

3.3 High Pressure Compressor

The coolant pressure is supplied from the 290 psi compressor in the turbine blade research lab. The compressor is a two stage, oil-injected screw compressor designed for higher-pressure air application from 13 bar up to 20 bar. With a two-stage design, both low and high pressure elements are built onto the gearbox driven by a highly efficient TEFC electric motor (IP-55, Class F insulation).



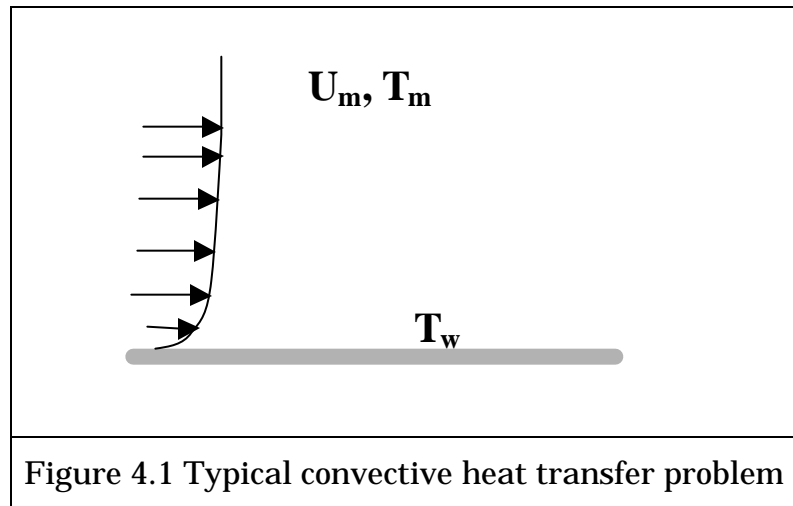
Figure 3.5 The high-pressure compressor

Chapter 4

Theory and Data Reduction

4.1 Heat Transfer Theory

As mentioned in chapter 1, this study will determine the local convection heat transfer coefficient of each pixel in the test section using a 1-D semi-infinite solid assumption. But to start with, let us define the heat convection part. The simple example to start with is a flow over a flat plate (figure 4.1). The local heat transfer flux is



$$q'' = h(T_m - T_w) \quad (4-1)$$

Where h is local heat transfer coefficient, T_m is the fluid temperature in contact with plate surface and T_w is the wall surface temperature. This equation has four variables. If h is to be computed, then the remaining three variables T_m , T_w and q'' are to be measured. Note that T_m and T_w maybe easy to measure but q'' is not. As assumed above (1-D semi-

infinite solid) the 1-D transient conduction equation, the initial condition and the convective boundary condition on the liquid crystal coated surface are

$$k \frac{\partial^2 T}{\partial x^2} = \rho c_p \frac{\partial T}{\partial t} \quad (4-2)$$

$$\text{at } t=0 \rightarrow T=T_i \quad (4-3)$$

$$\text{at } x=0, \quad -k \frac{\partial T}{\partial x} = h(T_w - T_m); \text{ as } x \rightarrow \infty, \quad T=T_i \quad (4-4)$$

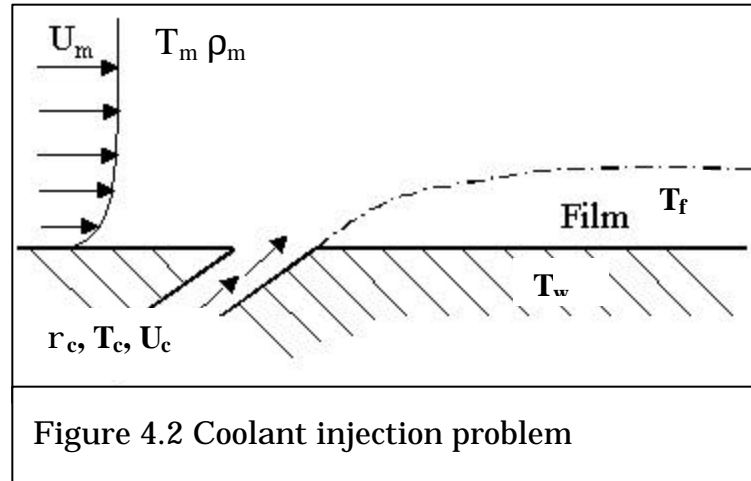
Equation (4-2) can be solved with the said conditions obtaining a non-dimensional temperature term at $x=0$ which is the convective boundary surface:

$$\frac{T_w - T_i}{T_m - T_i} = 1 - \exp\left(\frac{h^2 \mathbf{a} t}{k^2}\right) \operatorname{erfc}\left(\frac{h\sqrt{\mathbf{a} t}}{k}\right) \quad (4-5)$$

where (T_i) is the initial temperature of the test surface, (t) is time, (k) is the conductivity and (\mathbf{a}) is the thermal diffusivity (time constant). Note that if these are known, then the above equation will become solvable for (h). Thus, only a single equation maybe needed to compute a single value for (h). This might not be the case when the plate is being cooled by film injection.

Now let us consider our case where the coolant air is being injected from the bottom of the plate surface as shown in figure 4.2. Now in addition to the mainstream flow, we have a secondary flow. In this case we have three different temperatures to consider T_m , T_w and T_c . The last temperature is the coolant temperature. But even these temperatures

don't address the problem completely as the temperature difference term in equation (4-1) needs the local temperature. That local temperature may be referred to as T_f or film temperature. From which the local heat transfer flux is represented by



$$q'' = h(T_f - T_w) \quad (4-6)$$

It is reasonable that the local heat flux going into the surface has to pass through the film, therefore the new term T_f must be measured. This temperature is the result of mixing the hot stream and coolant jet and is expected to be in range of $T_m > T_f > T_c$. To obtain the film temperature, the ratio of the main fluid to secondary fluid is to be defined as follows

$$h = \frac{T_f - T_m}{T_c - T_m} \quad (4-7)$$

The term (η) is referred to as film effectiveness. The maximum value this term could take is 1 and that it is when the film temperature is equal the coolant temperature. This theoretical scenario implies that the film is 100% effective. In contrast, the film effectiveness is worst ($\eta=0$) when the temperature of the film is equal to the main, hot, stream.

The local convective heat transfer coefficient for the film cooling case is obtained using the same approach as for the simple case, where no film is applied; therefore equation (4-5) can be used with modifications. In fact the only change would be replacing the mainstream temperature T_m with the film temperature T_f . To find T_f , we will use equation (4-7) expressing is as:

$$T_f = \mathbf{h}(T_c - T_m) + T_m \quad (4.8)$$

$$T_f = \mathbf{h}T_c + (1 - \mathbf{h})T_m \quad (4.9)$$

Now it should be apparent that the main equation (4-5) could be applied with substituting T_m with T_f using (4-9). The resulting term will be

$$T_w - T_i = \left\{ 1 - \exp\left(\frac{h^2 \mathbf{a}t}{k^2}\right) \operatorname{erfc}\left(\frac{h\sqrt{\mathbf{a}t}}{k}\right) \right\} \{\mathbf{h}T_c + (1 - \mathbf{h})T_m - T_i\} \quad (4.10)$$

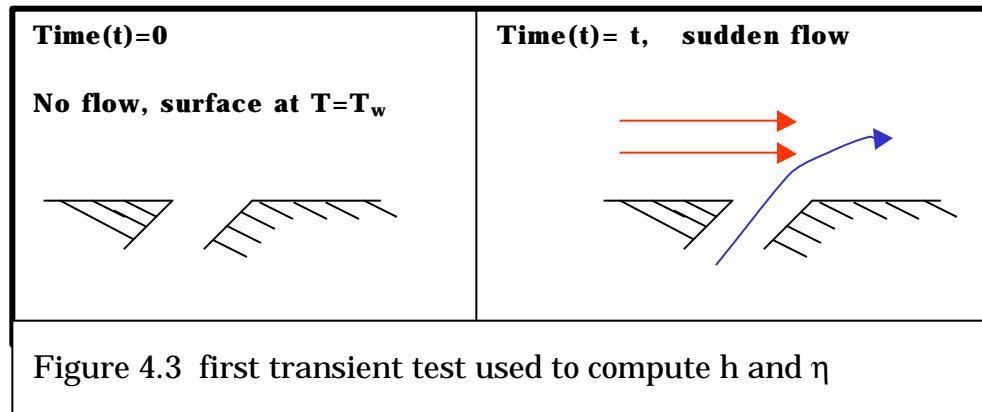
The last equation is a function of two unknowns, (h) and the (\mathbf{h}). Note that (\mathbf{h}) is defined in terms of T_f . This means the film temperature is solved for if the effectiveness is

obtained. Two equations are required to obtain the value of local heat transfer coefficient and film effectiveness.

4.2 Data Reduction

To produce two equations, two tests have to be conducted to supply the desired data to calculate the (h) and (η) . The transient tests are explained as follows:

- (i) The hot test: in which the mainstream flow is heated to a certain temperature within the band calibration range of the liquid crystal sheets used for test plate. The test plate is kept at ambient temperature. The coolant is kept at low or ambient temperature. When the temperatures of both the mainstream and coolant are stable then the test starts by suddenly imposing both the coolant and hot mainstream flows, (see figure 4.3), on the plate surface.



- (ii) The second test is no different than the first except that the coolant is also heated to a temperature within the calibration range of the liquid crystal sheets covering the test plate. As in test 1, the test plate is kept at ambient temperature. The reason for heating the coolant is to create different conditions that will help producing a distinct second equation.

For both tests, once the hot stream passes over the test section, its temperature does not raise as true step change but rather in gradual fashion. This gradual raise in temperature is accurately recorded. All these temperatures are functions of the time. The temperature are represented as a series of time step changes (ϕ_j , $j=1, 2, \dots, N$). Using superposition, the solution of both tests can be obtained from equation (4-10) as:

$$T_w - T_{i_1} = \sum_{j=1}^N \left\{ 1 - \exp\left(\frac{h^2 \mathbf{a}(t_1 - \mathbf{f}_j)}{k^2}\right) \operatorname{erfc}\left(\frac{h\sqrt{\mathbf{a}(t_1 - \mathbf{f}_j)}}{k}\right) \right\} \{ \mathbf{h}T_{c1} + (1 - \mathbf{h})(\Delta T_{m1})_j \} \quad (4-11)$$

$$T_w - T_{i_2} = \sum_{j=1}^N \left\{ 1 - \exp\left(\frac{h^2 \mathbf{a}(t_2 - \mathbf{f}_j)}{k^2}\right) \operatorname{erfc}\left(\frac{h\sqrt{\mathbf{a}(t_2 - \mathbf{f}_j)}}{k}\right) \right\} \{ \mathbf{h}(\Delta T_{c2})_j + (1 - \mathbf{h})(\Delta T_{m2})_j \} \quad (4-12)$$

Equation (4-11) above is addressed in terms of the step change in mainstream temperature ΔT_m while equation (4-12) includes the step change in coolant temperature ΔT_c . Note the term representing the initial temperature is included in the first step change ΔT_{m1} for $j=1$. For a maximum set error of (1/1000,000), the two equations are solved by iteration using a standard mathematical subroutine.

Based on the methodology of Kline and McClintock (1953), the uncertainty of these calculations are preformed. The individual uncertainties are listed below:

$$\partial T_c = 2.0 \times 10^{-3} \quad \text{K} \quad (4-13)$$

$$\partial T_m = 2.00 \times 10^{-3} \quad \text{K} \quad (4-14)$$

$$\partial T_i = 0.027 \quad \text{K} \quad (4-15)$$

$$\partial t = 0.02 \quad \text{s} \quad (4-16)$$

$$\partial \mathbf{a} = 0.03 \quad \text{m}^2/\text{s} \quad (4-17)$$

$$\partial k = 0.03 \quad \text{W/mK} \quad (4-18)$$

The average overall percent error is $\pm 6.4\%$ for h and is $\pm 7.9\%$ for η . The highest error would be as high as 17% and is expected to appear in the area around the injection holes due to 2-D conduction.

Chapter 5

Results: Heat Transfer Measurements

5.1 Baseline Case

5.1.1 Span Averaged Heat Transfer Coefficient (h) (baseline)

As mentioned in chapter 3, five cases have been studied. Each case represents a distinct hole exit geometry. These geometries vary from normal 35° exit to angled slot. To help in analyzing the data and to establish a reference where all geometries can be compared to, the normal case was chosen to be the *baseline* for all other cases.

Figure 5.1 shows the average heat transfer coefficient (h) for the blowing ratio

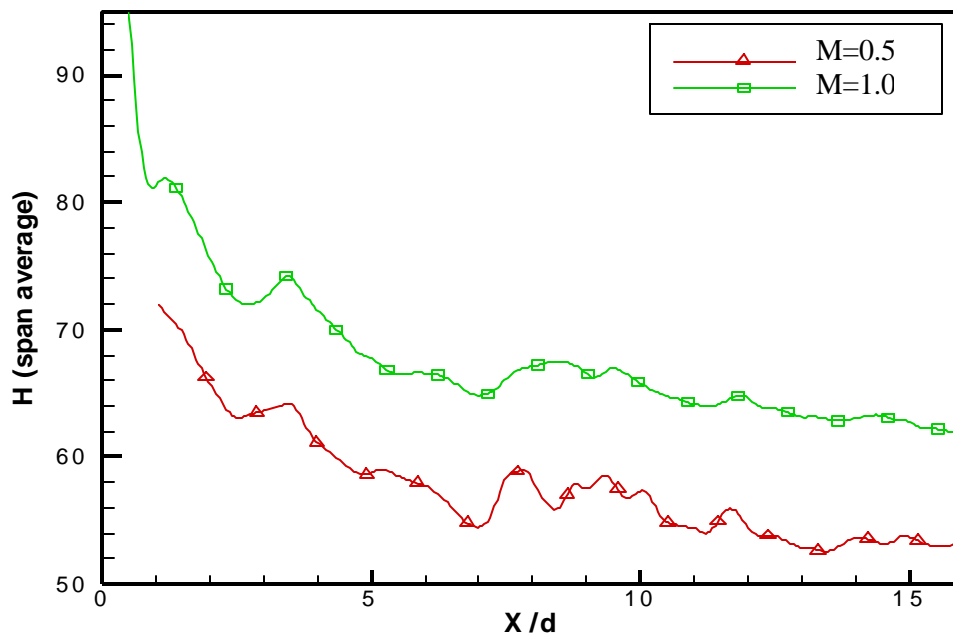


Figure 5.1 Baseline h for $M = 0.5$ & 1.0

$M = 0.5$ & 1.0 . The Figure representation is along the streamwise direction defined by the dimensionless term (X/d) , where X is the distance downstream the hole and d is the hole's diameter. The term "span" refer to the perpendicular direction to the streamwise as pointed in chapter 1. These original exact local values from which Figure 5.1 is obtained is shown in Figure 5.2. Although the average heat transfer coefficient is at its peak for near the holes, this value may not be considered. From the uncertainty analysis, the error is expected to be the highest, (17%) in this vicinity.

The most important indication of the Figure is the trend of the coefficient values from $X/d = 2$ to 16. The obtained curve is in general agreement with similar cases by Ekkad et al. (1997a). As expected, the trend for average heat transfer coefficient shows higher values with small X/d . It also posses small values or zero at large X/d . The X/d was limited to 16 because there is no significant comparison value for h is obtained after beyond 16 for the mainstream velocity. Note that X/d range will vary according to test conditions such as the mainstream velocity and the blowing ratio. For this study the mainstream velocity was fixed at 9 m/s throughout all cases. With mainstream velocity of 105 m/s, Bunker et al (2002) was able to produce readable range up to 100 X/d .

Figure 5.1 shows that the higher blowing ratio enhances the net heat exchanged between the plate surface and the mainstream and hence results in larger h for higher blowing ratio. This confirms with the results obtained by Ekkad et al (1997), and Bunker et al (2002). The local values h for the two blowing ratio are shown in Figure 5.2.

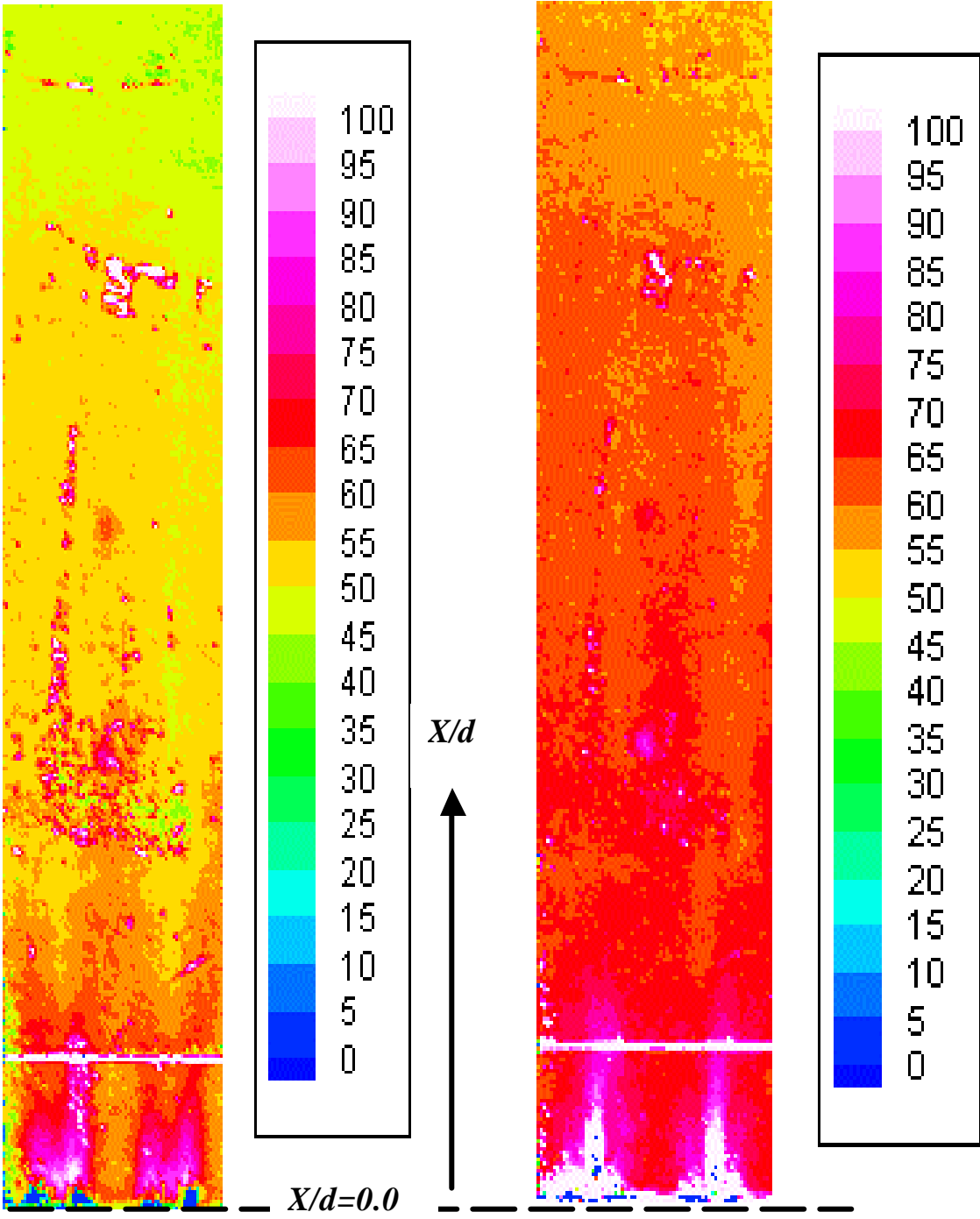


Figure 5.2 Local heat transfer coefficient for $M=0.5$ (left) and $M=1.0$ (right)

Figure 5.2 is obtained using equation (4-11). A close look at this Figure turn out the following comments:

- (i) The local heat transfer coefficient values near the holes are not representative of the actual coefficient. At some local areas, $X/d \ll 1.0$, the coefficient was less than $5 \text{ W/m}^2\cdot\text{K}$.
- (ii) Higher blowing ratio, $M=1.0$ in this case, results in an increases in the average h .
- (iii) In addition to (ii), the (X/d) range over which h has shown higher values is further extended for higher blowing ratio. This means that the net heat exchanged between the plate and mainstream was less effective in areas further than $X/d= 10$ for blowing ratio $M=0.5$.
- (iv) Along the hole jet centerline, h is found to be higher than other local areas.
- (v) There is a consistent difference of $\sim 10 \text{ W/m}^2\cdot\text{K}$ between spanaveraged h values for the two blowing ratios in the in the range $1.0 < X/d < 16.0$.
- (vi) The noise in some spots was filtered when computing the span average in Figure 5.1

5.1.2 Span Averaged Adiabatic Film Effectiveness (h) (Baseline)

Figure 5.3 shows the adiabatic film effectiveness for the normal case. As indicated in chapter 4, the film effectiveness is obtained from equation (4-12). Each single η value at any X/d represent the sum average of all span h 's. For $M=0.5$, the film effectiveness shows a decrease trend as X/d decreases. This corroborates with the literature data from Gritsch et al. (1997). Also, a trend comparison between the normal case for blowing ratio $M=1.0$ and a geometrically similar case by Ekkad et al.

Span Averaged Adiabatic Film Effectiveness

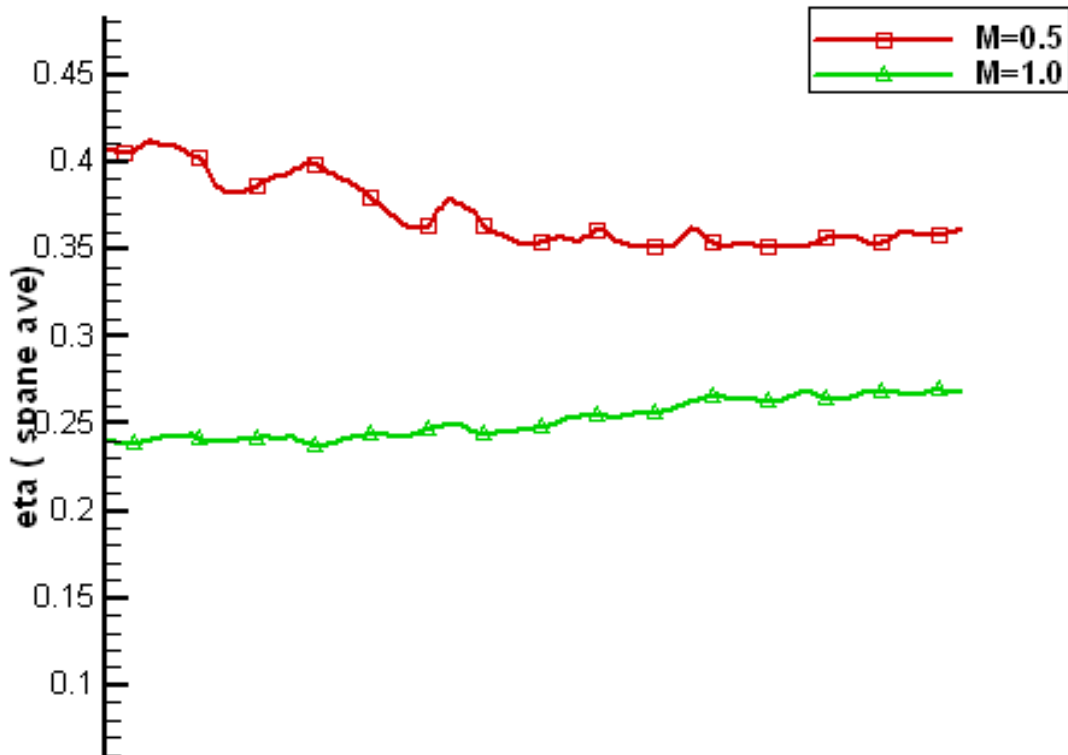


Figure 5.3 Baseline η for $M = 0.5$ & 1.0

(1997a) shows vast resemblance, as both tend to slightly increase with respect to X/d . In general, the film effectiveness curve drifts from a “declining” behavior to a slightly “growing” one as we increase the blowing ratio. This may indicate that, as we increase the blowing ratio, the coolant jet loses its ability to form an impenetrable film at the point of mixing with mainstream. Therefore, instead of bending over the surface, it impels to pound through the mainstream and then re-attach downstream the flow. This re-attachment could account for the slight increase in h at further X/d .

Figure 5.4 exhibits the local adiabatic film effectiveness values averaged in the spanwise direction. This Figure reveals some significant remarks that can be summarized in the following:

- (i) The jet centerline is associated with higher film effectiveness while almost no cooling effect in between holes for all ranges of X/d .
- (ii) The same logic in ignoring the local heat transfer coefficient values is applied here for film effectiveness just after the holes.
- (iii) Although it retained relatively higher value in heat transfer coefficient, the $M=1.0$ case shows poor film effectiveness. This could be seen clearly when compared to the case with $M=0.5$.
- (iv) The lower blowing jet for $M=0.5$ seemed to help maintaining the film coherence. This assumes the coolant jet was slow enough to be “pushed” along the streamwise direction rather than “penetrated.”
- (v) Even with the presence of data noise at some spots, the trail of the film could be tracked clearly, for $M=0.5$, till $X/d=16$ indicating a relative stability of the film compared to $M=1.0$.

As mentioned earlier, the film effectiveness and convective heat transfer coefficient obtained for normal case will be the baseline of the following cases. Therefore, they will be referred to as h_o and \mathbf{h}_o from this point forward.

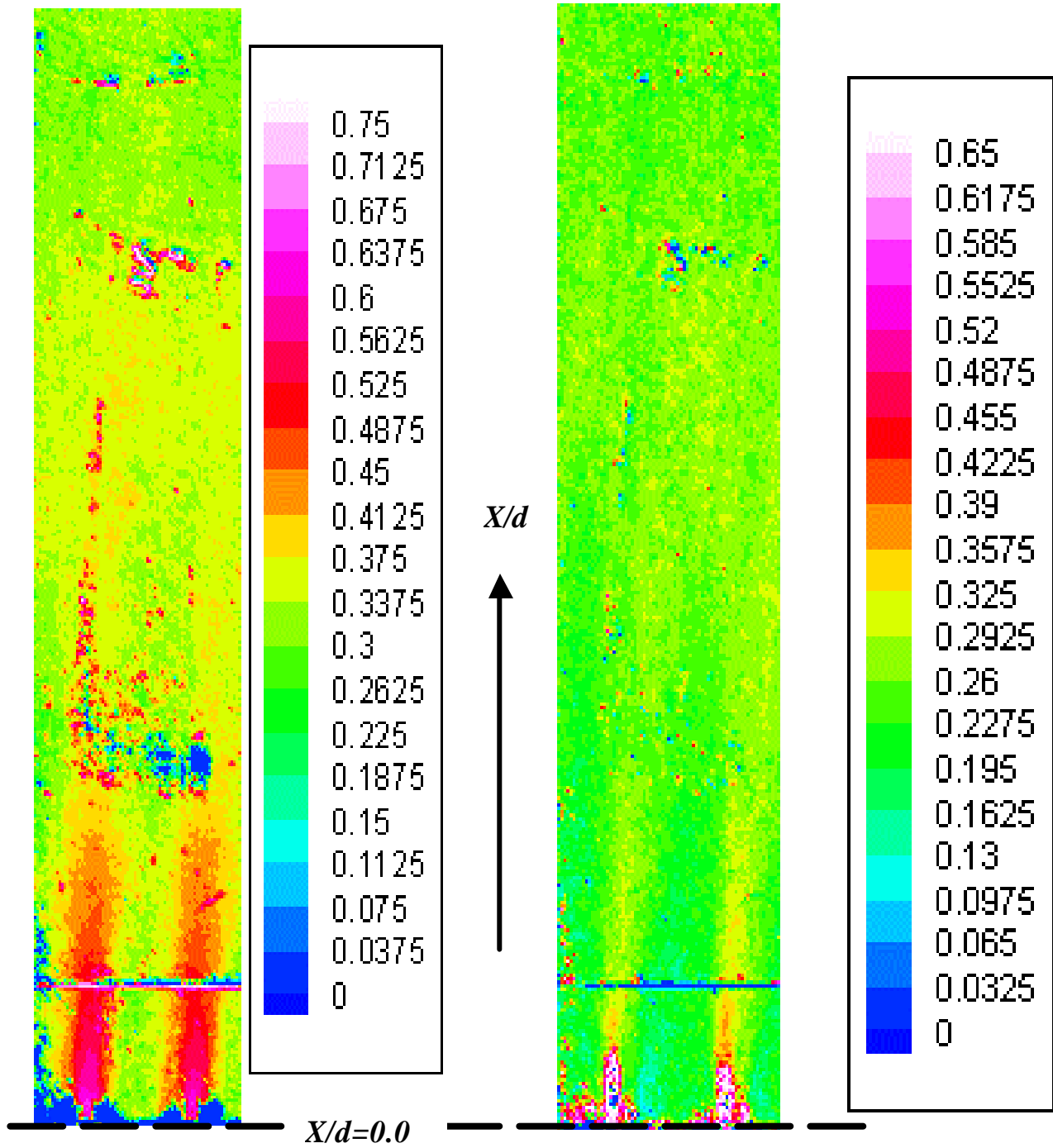


Figure 5.4 Local film effectiveness for $M=0.5$ (left) and $M=1.0$ (right)

5.2 Slot Case

The slot case is a 35 degree inclined hole, along the stream, sitting in a 1.75-inch wide and 0.2-inch high rectangular groove (see chapter 2). The span averaged h for the two blowing ratios is shown in Figure 5.5. Although these data are span-averaged, the local values are in consistency with them, as to be seen when analyzing Figure 5.9. Both blowing ratios demonstrate a high peak around $X/d = 3$. This peak is followed by moderately declining values of heat transfer coefficient. The peak is expected to be the result of the local turbulence following the immediate mixing of the two streams, the hot and the cold. This peak is common in almost all cases as to be seen next.

Increasing the blowing the ratio from 0.5 to 1.0 boosted the heat transfer coefficient with an average of 6-8 $\text{W/m}^2\cdot\text{K}$ for $X/d > 5$. Apart from this shift, it can be said that there is no significant enhancement to h at this case with respect to the change in blowing ratio M . Further look into Figure 5.6 provide a comparison between the performances of this geometry with reference the baseline. This Figure represents the normalized span-averaged heat transfer coefficients (h/h_o) for both blowing ratio. Unexpectedly, the lower blowing ratio case, in general, compared better with the normal case than $M= 1.0$.

Examining the results from Figures 5.7 –10 reveals the following comments:

- (i) In addition holding higher local heat transfer coefficient, the higher blowing ratio $M=1.0$ is also showing somewhat good film effectiveness.

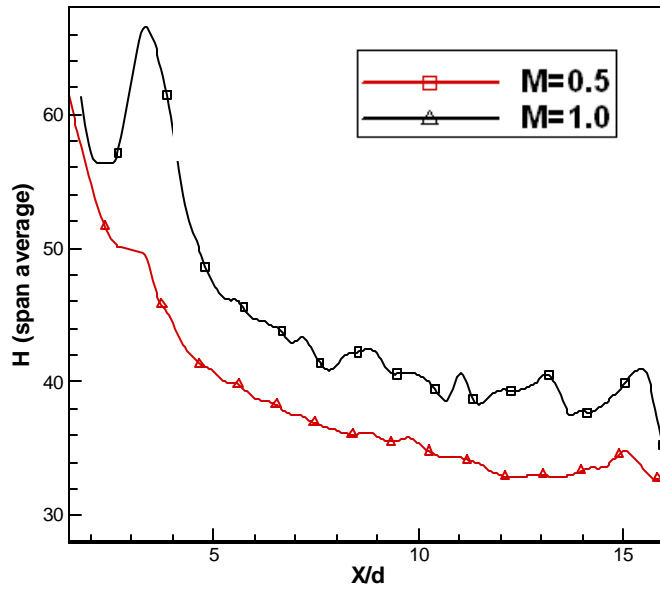


Figure 5.5 Average h for slot case

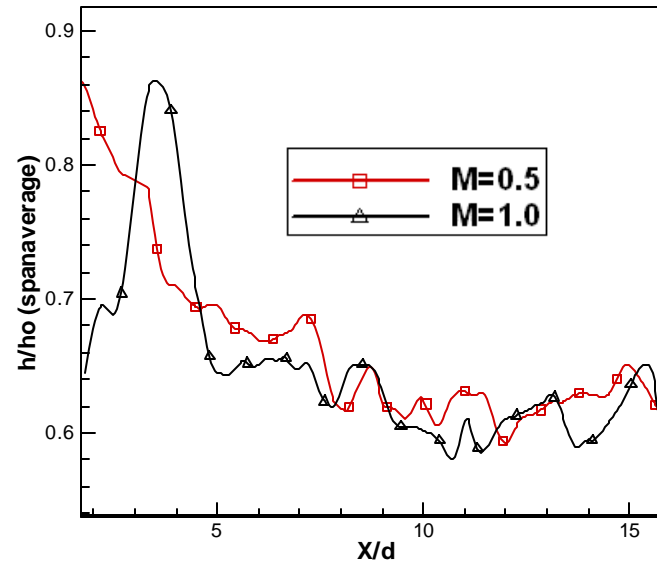


Figure 5.6 Normalized average h for slot case

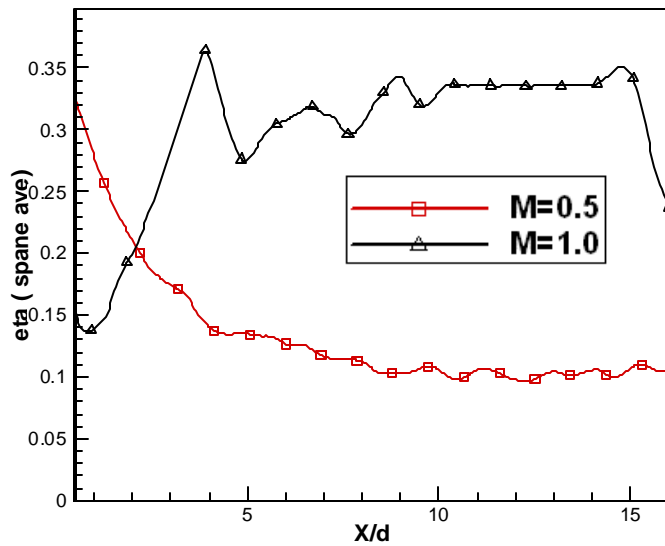


Figure 5.7 Averaged η for Slot case

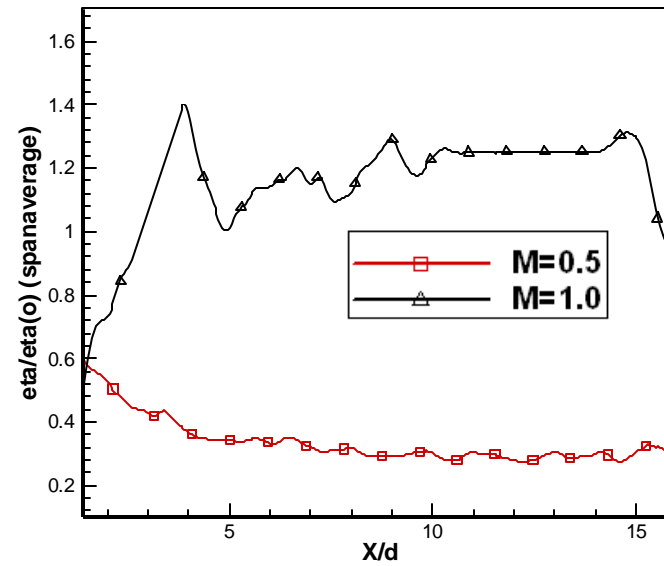
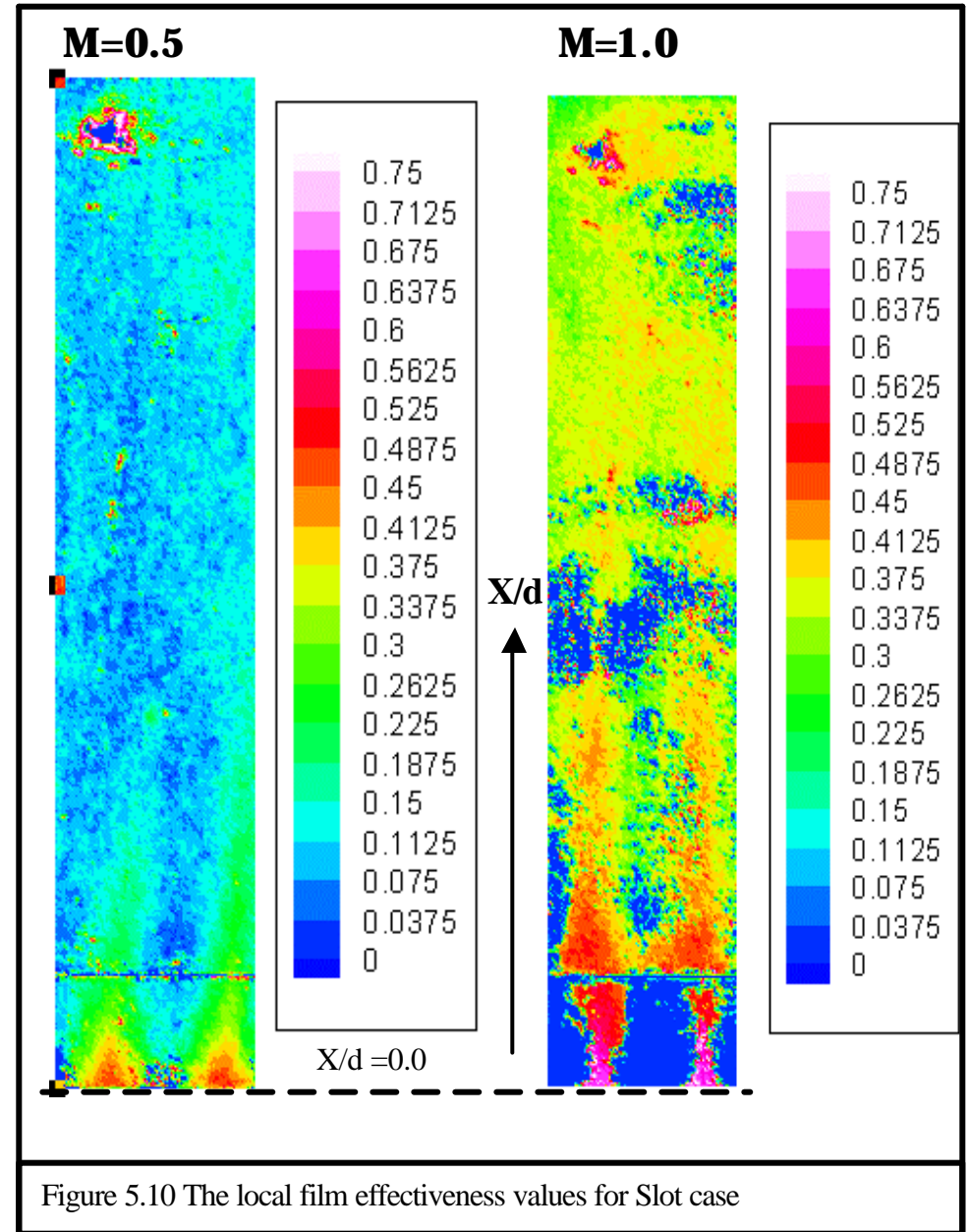
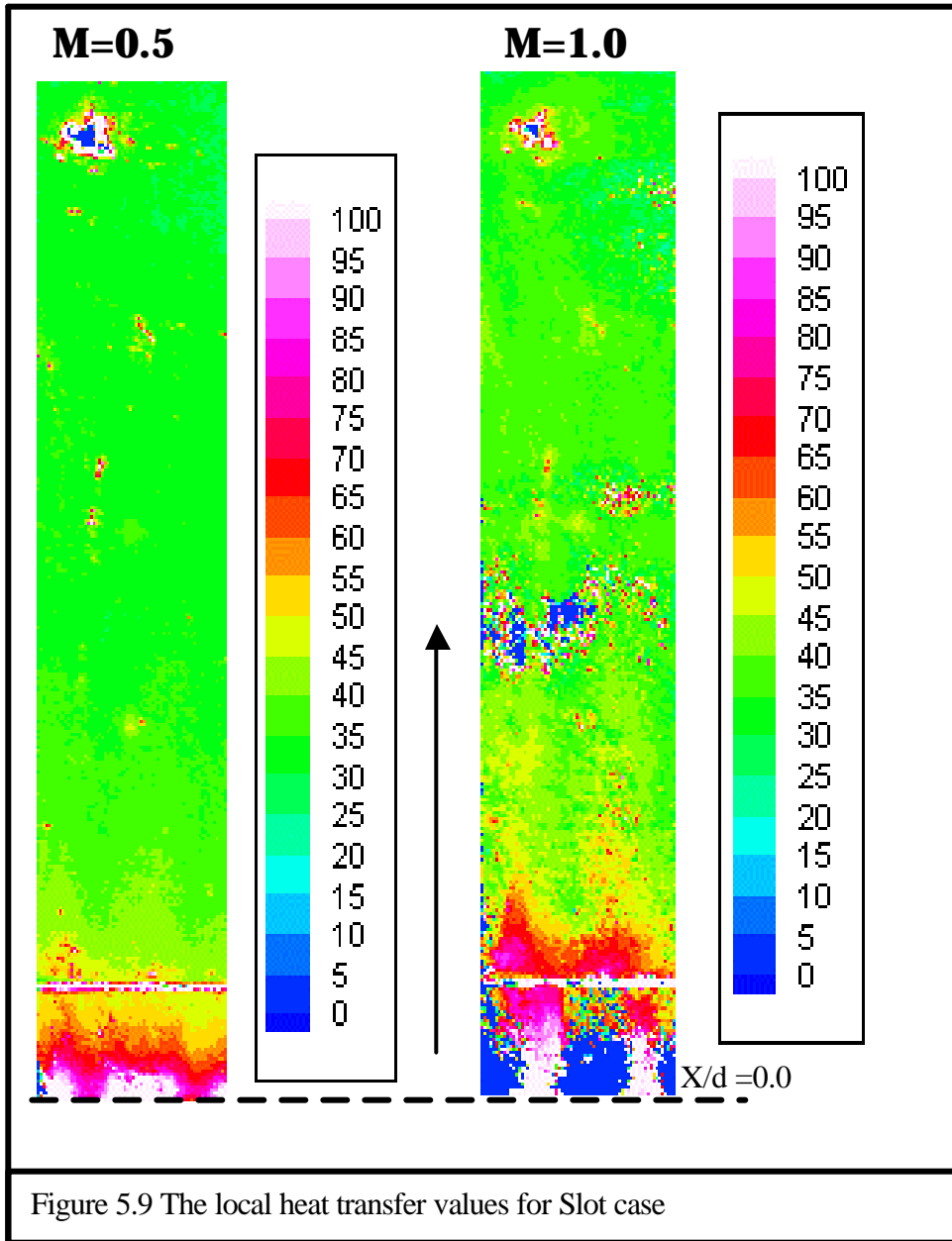


Figure 5.8 Normalized η for Slot case



- (ii) Point (i) can be visualized clearly in Figure 5.9 where the range of the normalized film effectiveness is always greater than 1.0 for $3.5 \leq X/d \leq 15$.
- (iii) The low blowing ratio case does not promote potentials for further investigation as its normalized heat transfer coefficient is higher or equal to that for $M=1.0$ and its normalized film effectiveness is mostly less than 0.4. This indicates its more effective to cool the surface with normal 35 degree hole rather than a slot type, for $M=0.5$.
- (iv) Figure 5.10 shows that film is present in the cooling jet centerline while there is almost no cooling taking place in between. This indicate narrow jet dispersion for $M=1.0$.
- (v) The film stability was not acceptable for $X/d < 5$ for the higher blowing ratio. It is essential to have a stable film to prevent local heat stress points or region. Figure 5.10 shows the local film effectiveness dropping to values less than 0.03 even within the jet centerline.
- (vi) In contrast, the lower blowing ratio posses more stable film, yet its value was not promising
- (vii) The instability of film in case of $M=1.0$ could be attributed to a secondary flow within the film itself resulting in film penetration at some X/d .

Both blowing ratio case cann't be compared with Bunker et al. (2002) as his blowing ratios were always 0.98 or greater. Also the velocity of the mainstream was much higher than 9 m/s resulting in 125 X/d range.

5.3 Double Shoulder Case

The double shoulder case is where the width of the slot is the same as hole diameter (0.5in). The flow in this case goes from 35° deg to 90° then merges with the mainstream (see chapter 2). The slot width to hole diameter ratio (W/d) = 1.0, which is the lowest possible value for W/d . Solving equation 4-11 and 4-12 for the double shoulder case will produce the local values for h and η shown in Figure 5.15 and 5.16. The span-averaged and normalized data are shown in Figures 5.11-14.

The very first thing to note was the insensitivity of this case, with regards to h , to the change in blowing. In fact, Figure 5.11 shows an almost identical behavior of $M=1.0$ and $M=0.5$. Although the lower was leading the higher with less than $3 \text{ W/m}^2\cdot\text{K}$, in average, both blowing ratios exhibits the same trend for the entire X/d range. Both have a relatively high heat transfer coefficient for the X/d less than 4. Among all geometries tested, the $M=0.5$ in this case scored the highest span-averaged heat transfer coefficient in the said range. This may not be desirable for the first glance, as we want to minimize the heat exchanged between the mainstream and the surface. But to perform a through case evaluation, we should also consider the film effectiveness. Examining the Figures in next pages provides the following comments:

- (i) For $M=0.5$, the double shoulder geometry, compared to the normal 35 degree, will always provide more heat exchanged between the blade surface and the hot mainstream for a distance less than $4 d$ downstream the hole exit.
- (ii) A similar argument can be made about the lower blowing ratio but for a shorter range, less than $2.5 X/d$.

- (iii) The adiabatic film effectiveness was lower than expected when the blowing ratio was increased. The $M=1.0$ was less than the $M=0.5$ by an average of 0.1-0.15 for $X/d > 2.0$.
- (iv) The higher the blowing ratio the less stable the film. This instability was observed in two main areas, the first was at around $X/d=5.0$ and the other was $X/d = 10$. This was associated with a very low η for both local and average areas. These areas seem to be the result of the coolant jet lifting off.
- (v) The same lifting off behavior was also observed for the lower blowing ratio but with less effect. This implies that the $M=0.5$ produces better and more stable film than $M=1.0$.
- (vi) There is almost no cooling (see Figure 5.16) taking place in-between holes for $X/d < 4.0$ for both cases. Yet the lower the blowing ratio cooling jet starts dispersing after $X/d=6.0$ covering an appreciable portion of the surface. Locally, the maximum values of the film for this case was observed along centerline of cooling jet exiting the hole.
- (vii) Although its normalized film effectiveness values were barely above 1.0, the high blowing ratio does not show good potential as an optimum geometry. This is due to the fact that its film was not stable, in addition to its relatively high h .
- (viii) In contrast, the lower blowing ratio could be better choice for improved cooling as its net heat exchanged was less than that in the baseline for all $X/d > 2.0$. Also its film effectiveness factor was always above than the normal case with marginal values less than 0.1.

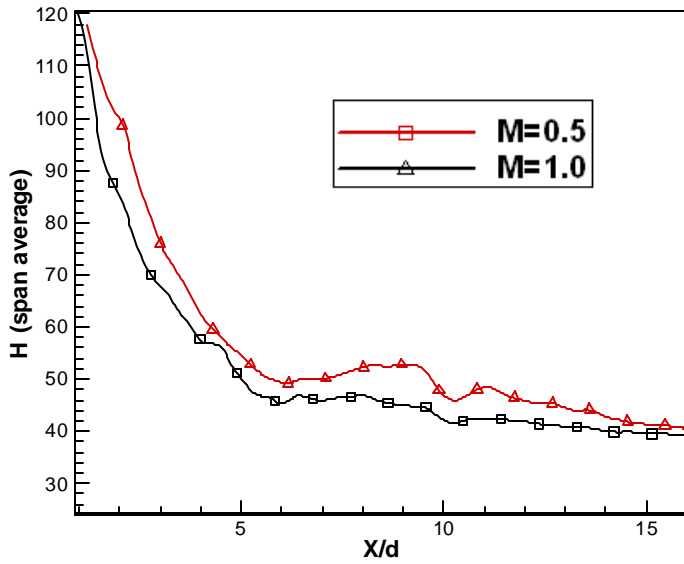


Figure 5.11 Average h for double shoulder

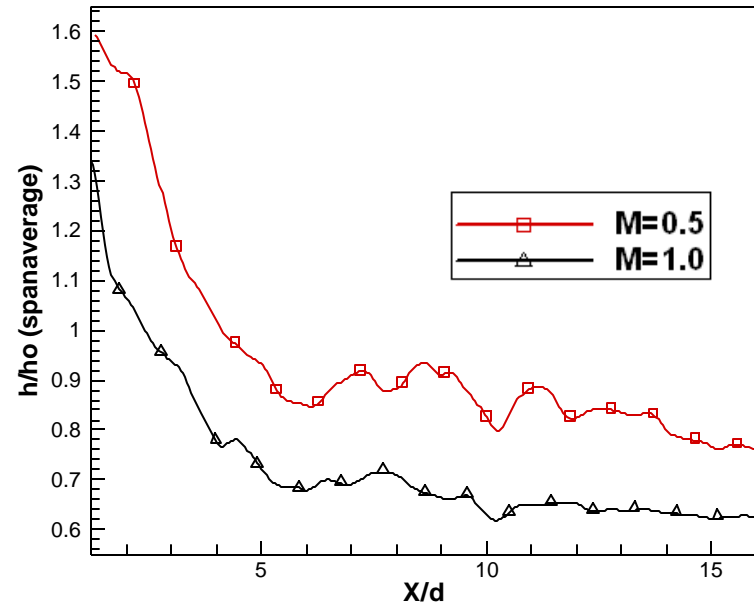


Figure 5.12 Normalized average h for double shoulder

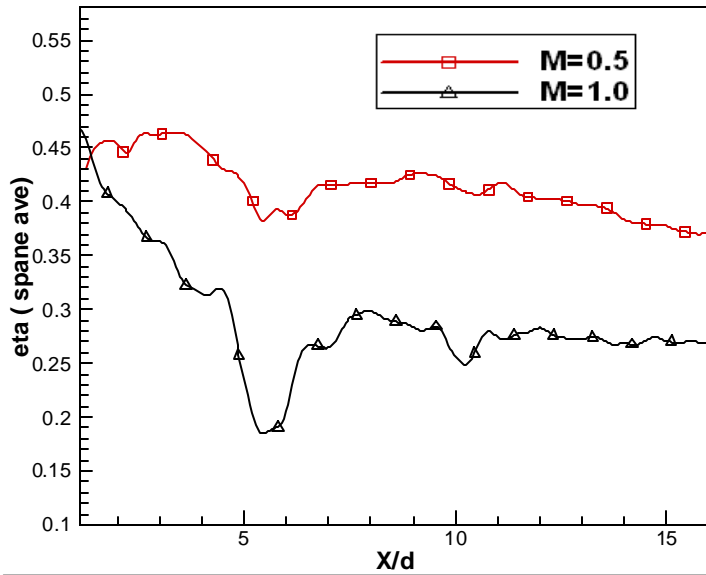


Figure 5.13 Averaged h for double shoulder

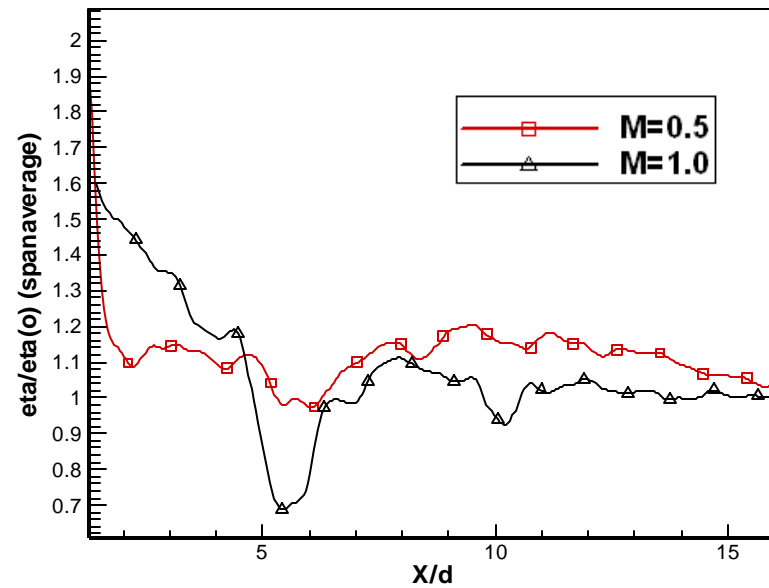


Figure 5.14 Normalized η for Slot case

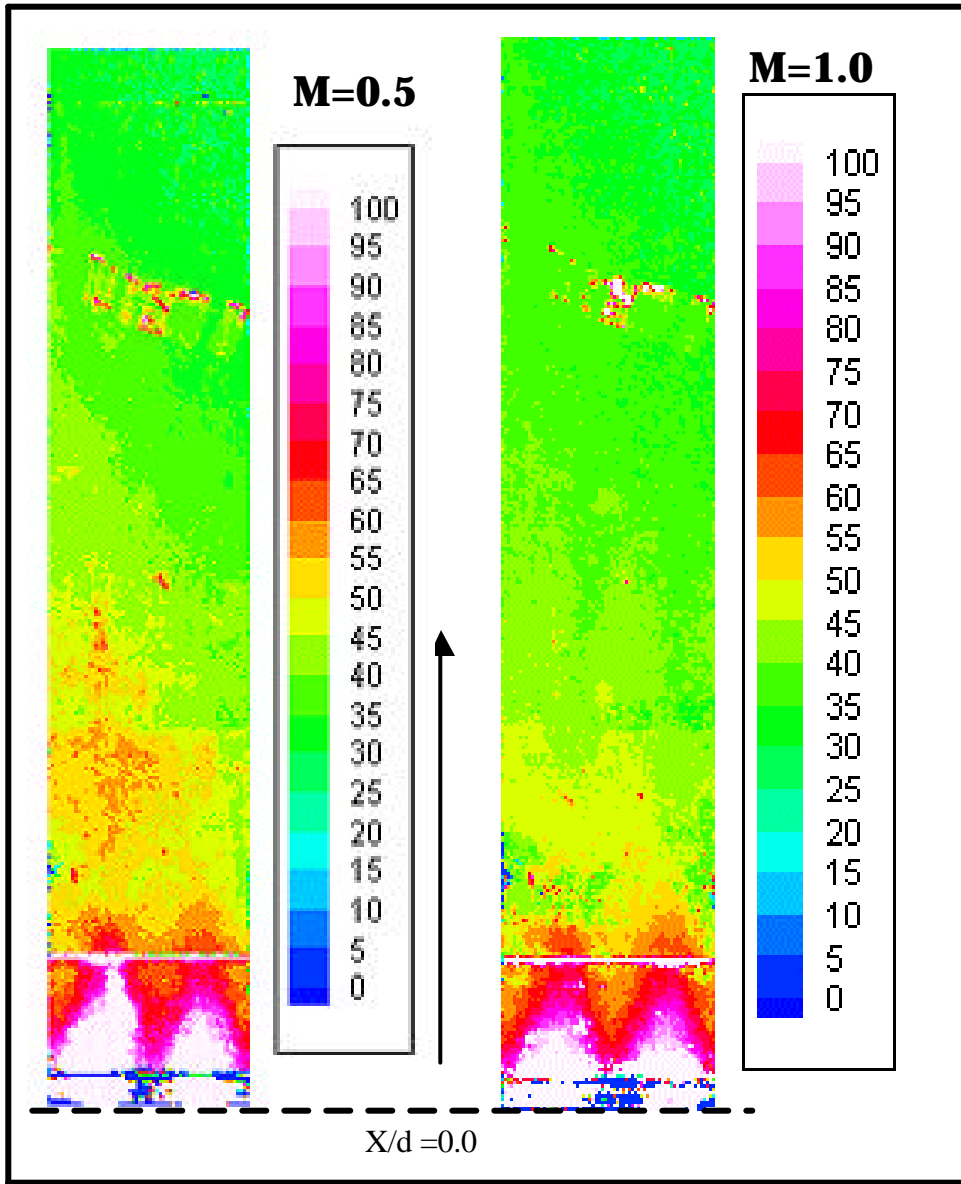


Figure 5.15 The local heat transfer values for Double shoulder case

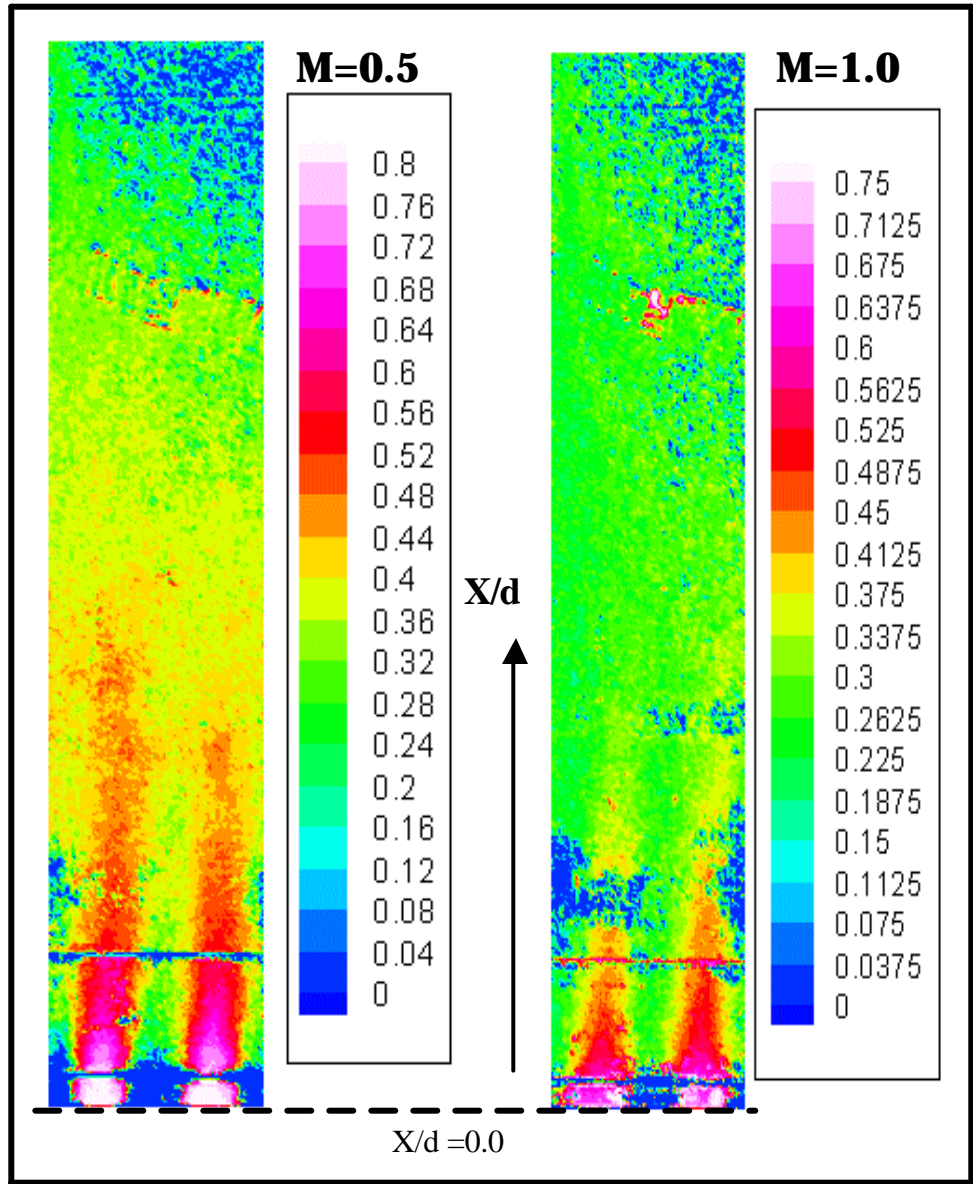


Figure 5.16 The local film effectiveness values for Double shoulder

5.4 Right Shoulder Case

As explained in chapter 2, the right shoulder case is similar to the slot case two except the width of the slot is 1.125in. The (p/d) ratio is still 0.4. The slot width to hole diameter ratio $(W/d) = 1.375$. Figure 5.17 and Figure 5.18 provide valuable information about the heat transfer coefficient for this geometry. The first Figure illustrates the span averaged h with respect to X/d . The two blowing ratios tested in this case show the regular trend of the convective heat transfer coefficient. Both start with high values, more than $85 \text{ W/m}^2\cdot\text{K}$, and gradually they lean to decrease with steady state finish line. The higher blowing ratio is leading the lower one with more $30 \text{ W/m}^2\cdot\text{K}$ for X/d less than 5. The difference reduces to an average of $16 \text{ W/m}^2\cdot\text{K}$ for remaining X/d . This is comparatively a high difference and for this study in particular is the highest. This indicates that this geometry is sensitive, for h , to flow change from the coolant as we change the blowing ratio. Figure 5.17 addresses the span-average comparison between this case and the baseline. The blowing ratio $M=1.0$, is higher than unity only for $X/d > 5.0$., then it drops progressively till it reaches 0.8 at $X/d=16$. The Low blowing ratio $M=0.5$ has been always better than the baseline case for the entire range. With values starting at 0.9 and declining to 0.6 at $X/d=16$, it is evident the low blowing ratio case for this geometry will exchange less energy and thus hold lower h than the baseline case. However this might not be enough to comprehensively evaluate the geometry. We still need to further examine the behavior of the film effectiveness make a better judgment.

Inspecting Figures 5.19-22 will disclose more information on how the average and local film effectiveness compare to the baseline. It will also reveal the nature of the film behavior on certain areas. On that regard the following comments are offered:

- (i) The low blowing ratio is associated with moderately good film effectiveness, around 0.45, for X/d less than 1.5. Then, rapidly the effectiveness drops to 0.2 and eventually to 0.1.
- (ii) Unexpectedly, the normalized film effectiveness $\frac{h}{h_o}$ is less than unity for entire range of X/d . With its value ranging between 0.6 and 0.4, the low blowing ratio does not seem to be a better geometry choice than the baseline case.
- (iii) The normalized film effectiveness values for high blowing ratio reveal interesting potentials for the double shoulder geometry. All span-averaged $\frac{h}{h_o}$ are higher than unity for entire range. In fact the values are unbeatably higher than all other geometries tested in this study. The curve starts at more than 1.75 and finishes up with slightly more than 1.2.
- (iv) This indicates that the right shoulder geometry with $M=1.0$ will definitely provide better cooling than the baseline case. It will also provide better protection, as its film effectiveness factor is higher than the baseline case.
- (v) Despite the fact the film effectiveness values are associated locally with cooling jet centerline, the high blowing ratio case shows the best cooling jet dispersion among all tested cases. With uniform jet scattering as shows in Figure 5.22, the higher blowing ration case covers almost all the range for $X/d=16$.

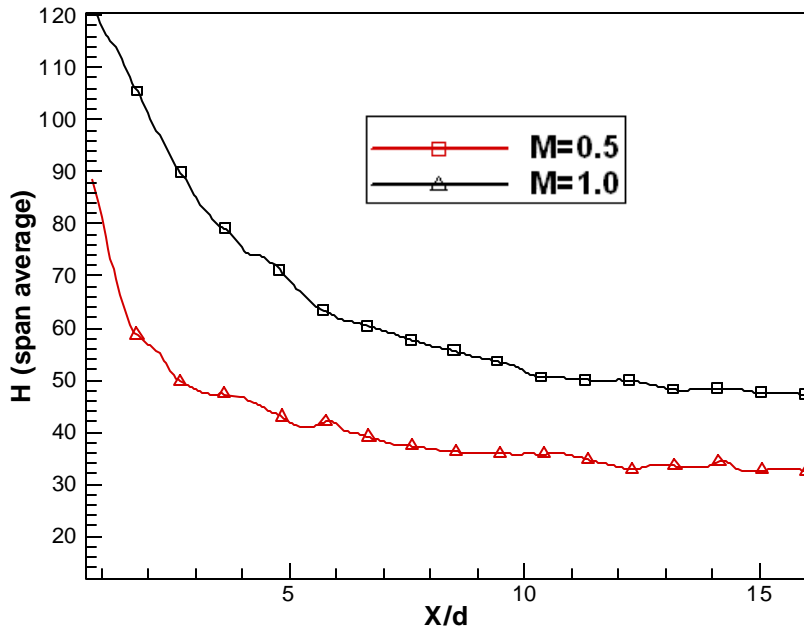


Figure 5.17 Average h for right shoulder

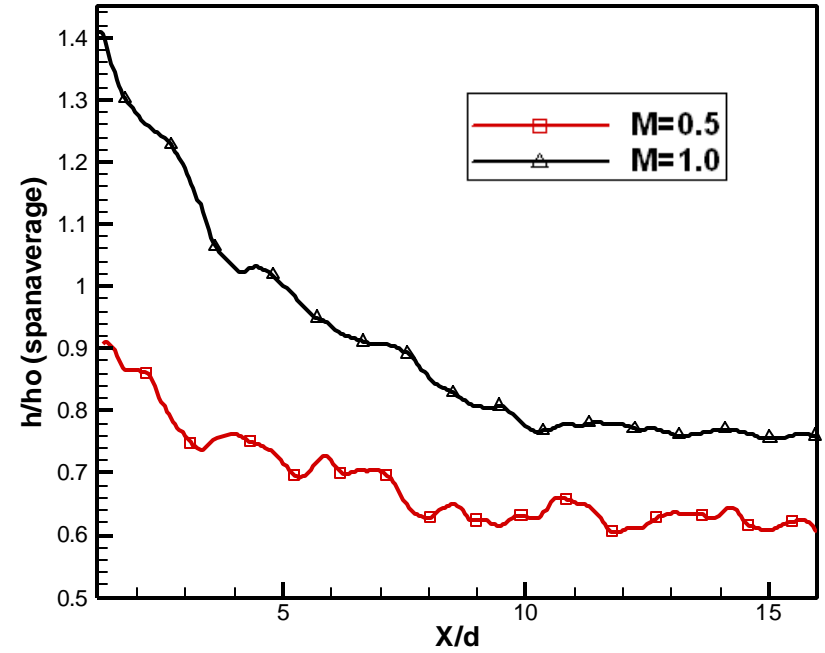


Figure 5.18 Normalized average h for for right shoulder

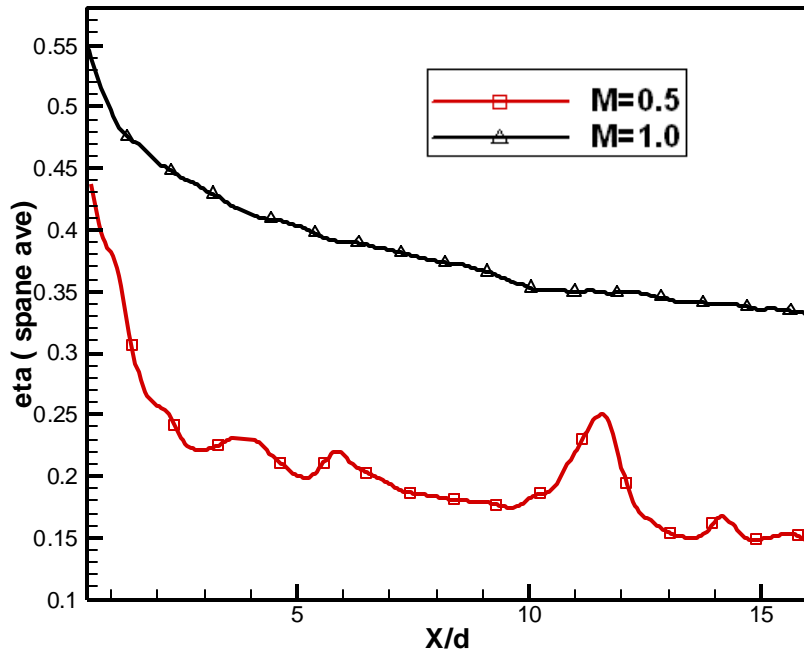


Figure 5.19 Averaged h for right shoulder

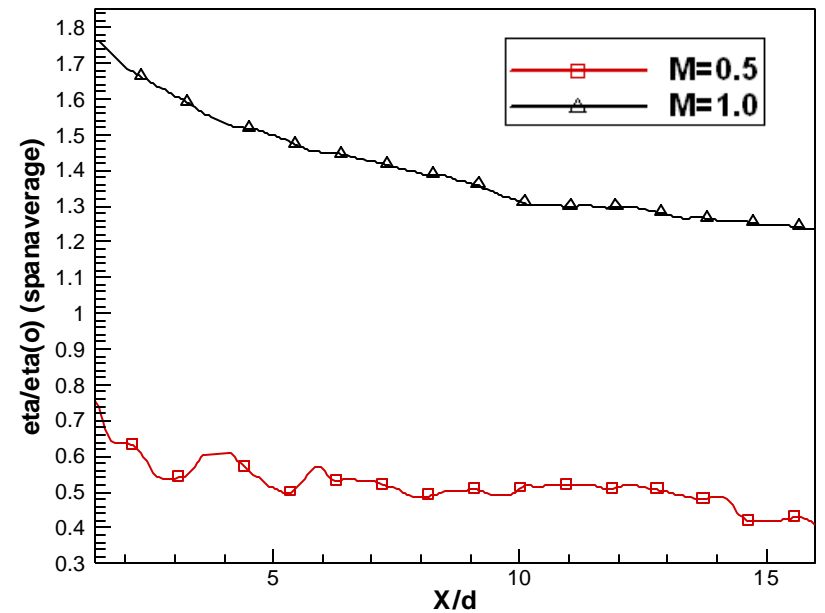


Figure 5.20 Normalized η for right shoulder case

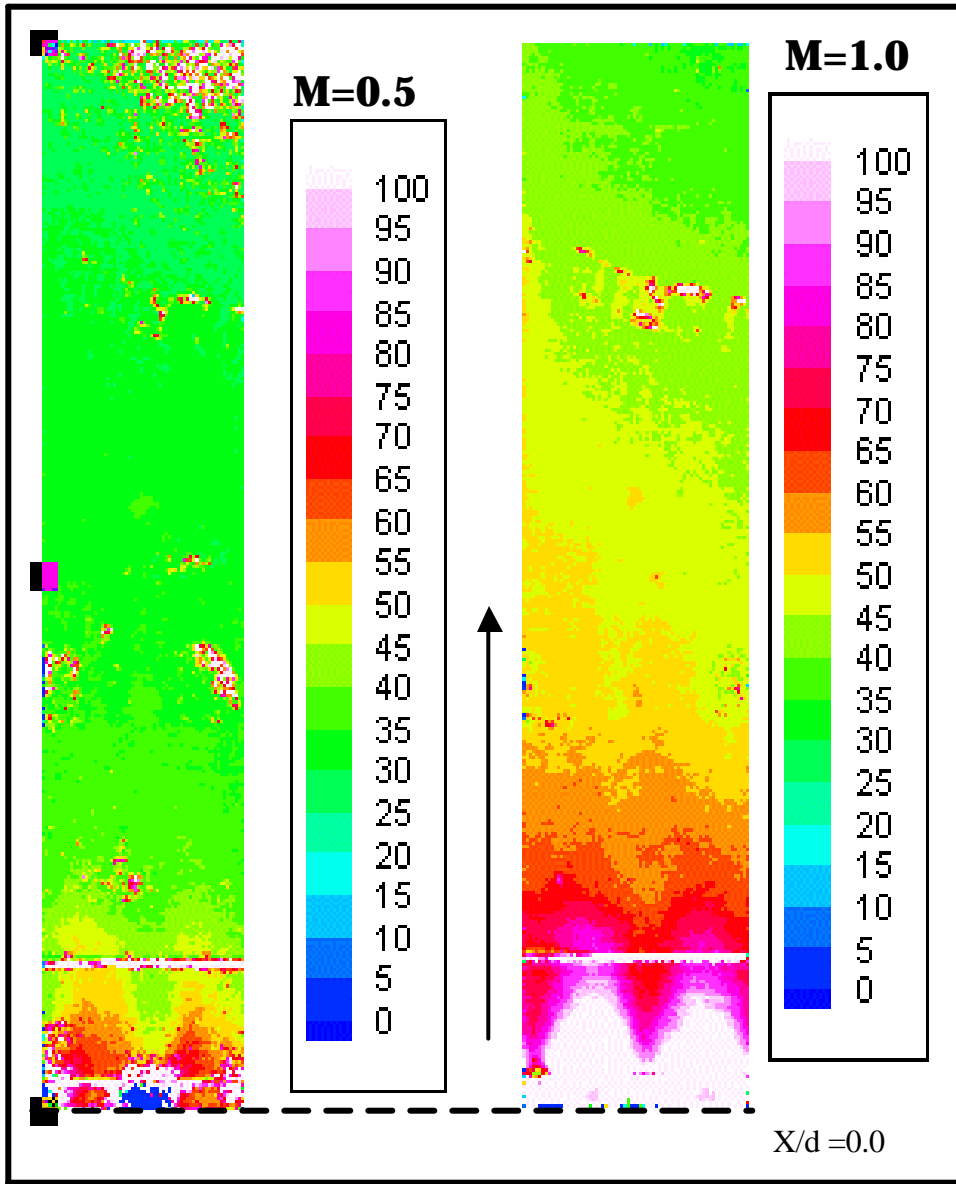


Figure 5.21 The local heat transfer values for Right shoulder case

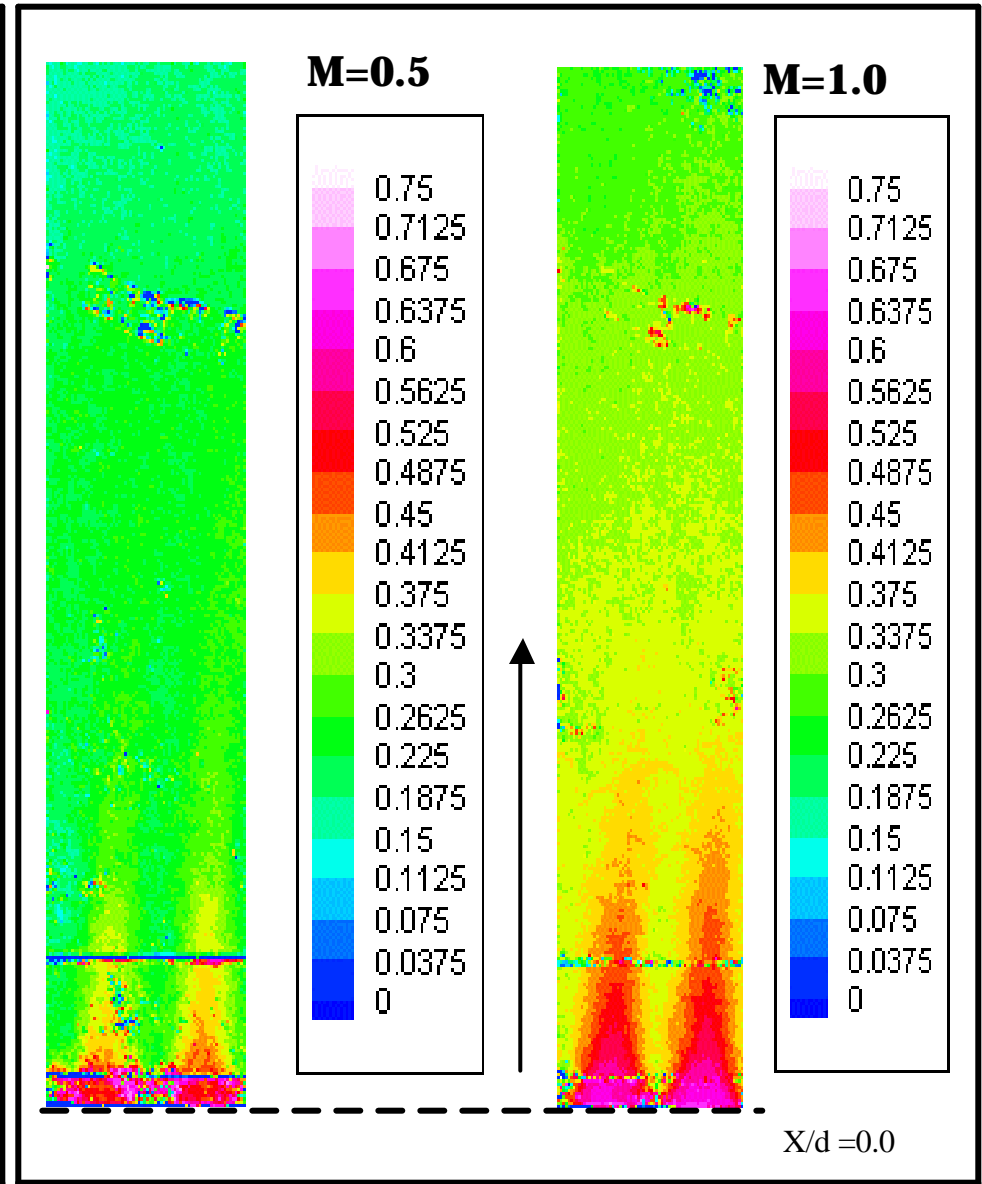


Figure 5.22 The local film effectiveness values for Right shoulder case

5.5 Angled Case

The angled case is originally a slot case geometry with the right attachment slanted with 18° slope. The (p/d) ratio is 0.4. The slot width to hole diameter ratio (W/d) is varying from 1.0 to 1.375. The initial expectations of this case was that the right attachment will provide a gradual introduction of coolant jet without penetrating the mainstream flow, which should result in better adiabatic film effectiveness and hence less net convective heat exchange transfer between the hot mainstream and the blade surface. However, actual test data did not meet these expectations.

The span-averaged heat transfer coefficients in Figure 5.23 indicate that the general trend of both blowing ratios is no different than most cases tested in this study. The interesting remark about this Figure is the average heat transfer coefficient values are less than the baseline case. The Figure shows that the expected initial peak was at less than $74 \text{ W/m}^2\cdot\text{K}$ for both is followed by the regular declining pattern that leads to a finishing line of less than $34 \text{ W/m}^2\cdot\text{K}$ the higher blowing and less than $30 \text{ W/m}^2\cdot\text{K}$ for the lower blowing ratio. With the exception of an up normal spike at $X/d= 2.0$, Figure 5.24 indicates that the normalized heat transfer coefficient for both blowing ratios were less than the expected.

There was no significant change in heat transfer coefficient when the blowing ratio was increased from 0.5 to 1.0. Even with the $6 \text{ W/m}^2\cdot\text{K}$ shift that the higher blowing ratio was leading the lower one, blowing ratios performed less than expected when compared to the baseline case in Figure 5.24. A meticulous investigation of Figures 5.25-28 reveals the following the comments:

- (i) The span-average film effectiveness values were relatively lower than the average of other cases.
- (ii) Opposite to the findings in Figure 5.23, the angled case is “flow” sensitive. This means that the change in the blowing ratio M reflects a noticeable change in the film effectiveness values.
- (iii) Both blowing ratios don’t show potentials for an optimum case as both possess low film effectiveness values that are less than the average of the tested cases.
- (iv) The local heat transfer coefficient is very low for $X/d > 5.0$. This is observed in both blowing ratios
- (v) The normalized film effectiveness values in Figure 5.26 confirm that both blowing ratios are not good enough to compete with the other geometries.
- (vi) When examining the local values in Figure 5.28, there is almost no cooling in-between the holes. Only the jet centerline held the highest film effectiveness
- (vii) Surprisingly, the angled case is one of the best-tested cases for film stability. Yet this stability is not good enough to provide optimum cooling.
- (viii) Both cases show poor jet dispersion as the high film effectiveness were observed in the cooling jet centerline.

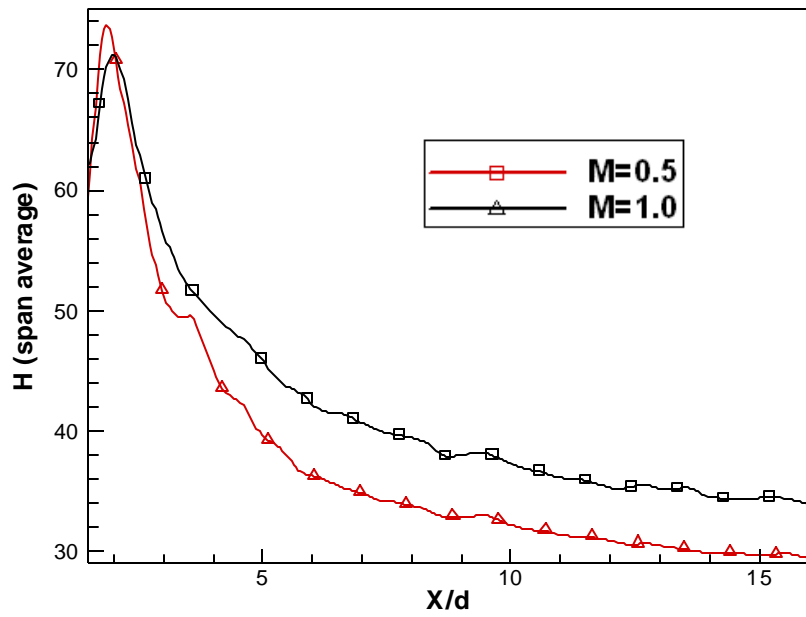


Figure 5.23 Average h for Angled case

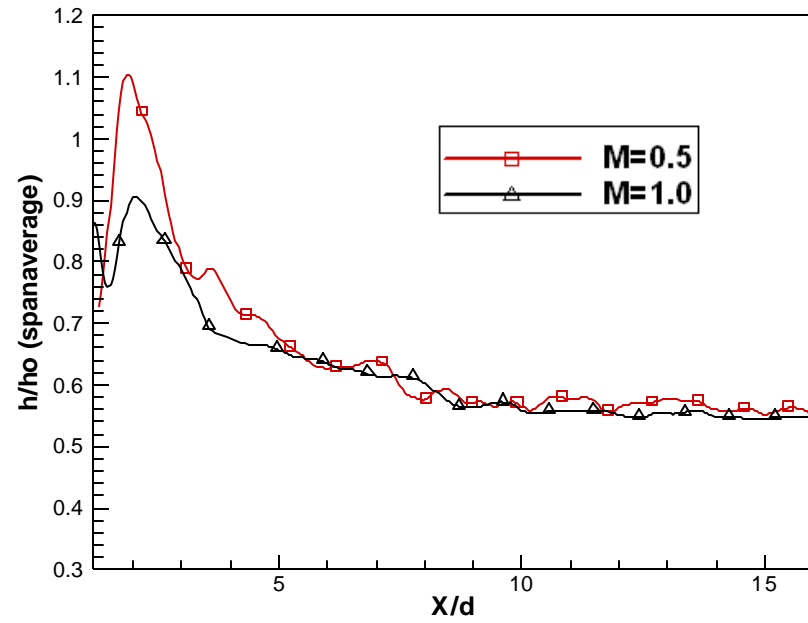


Figure 5.24 Normalized average h for Angled case

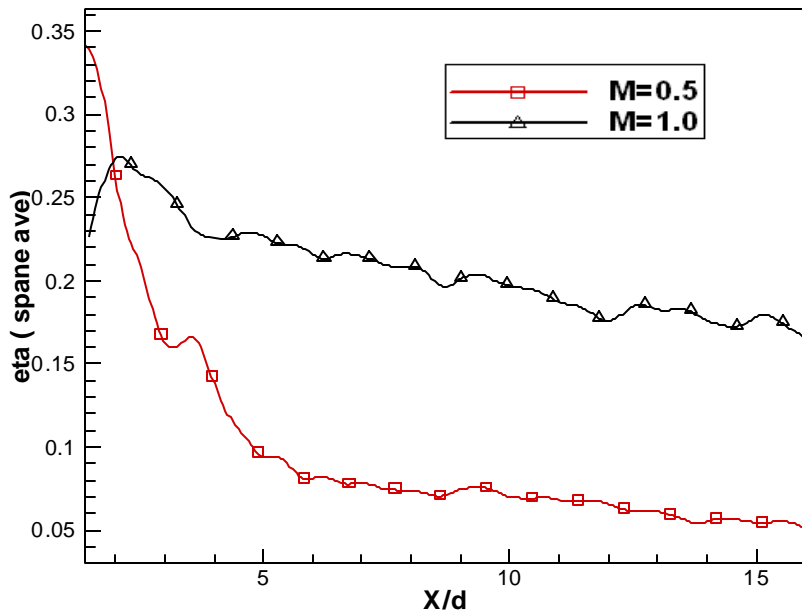


Figure 5.25 Averaged h for angled case

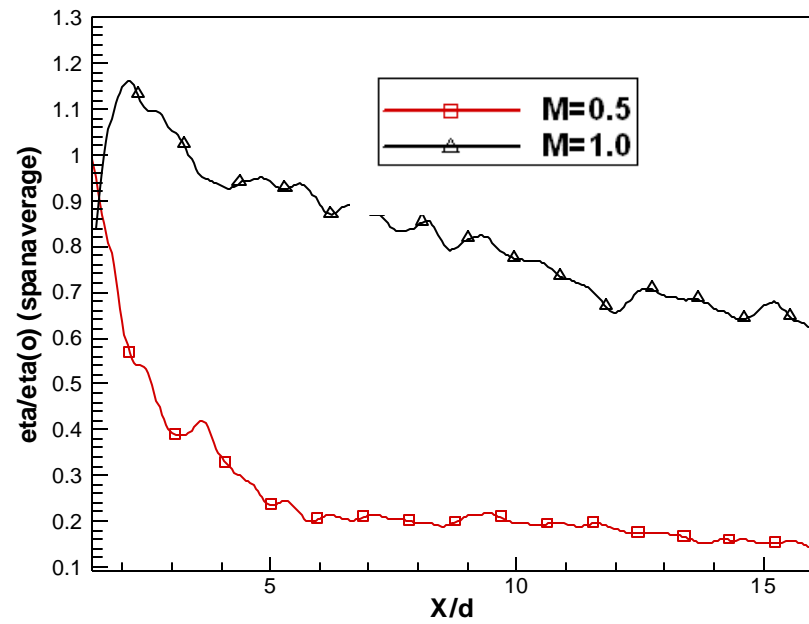
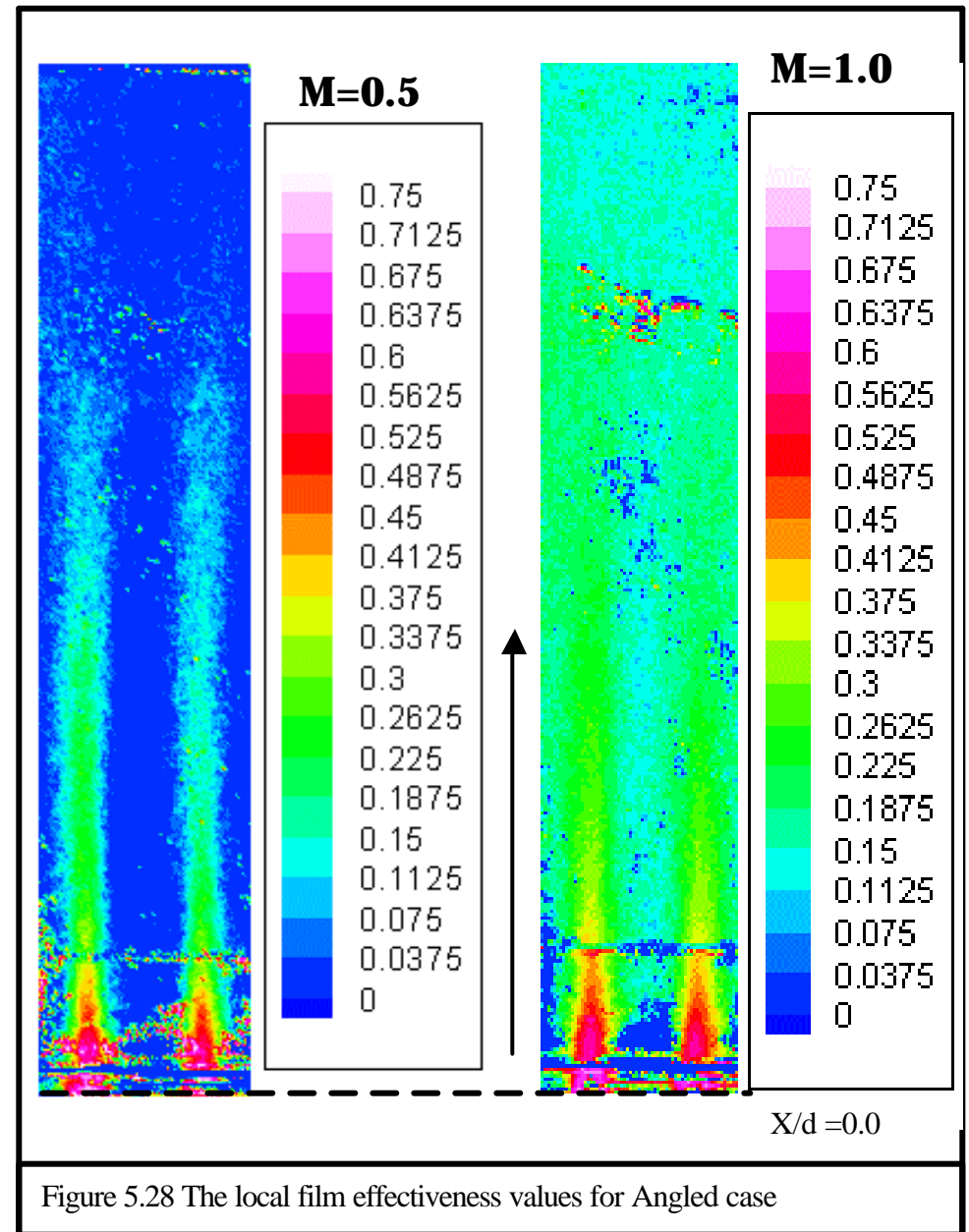
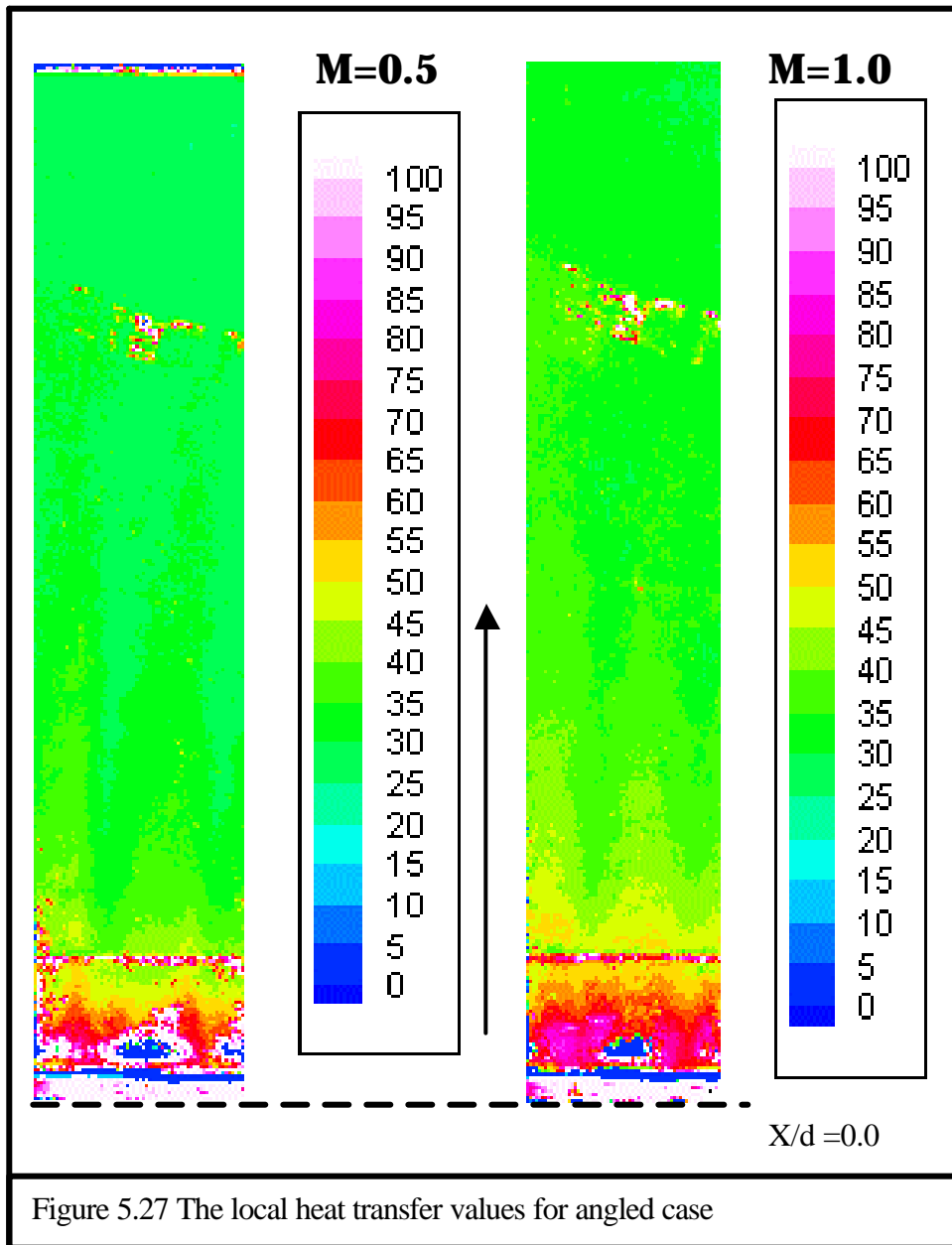
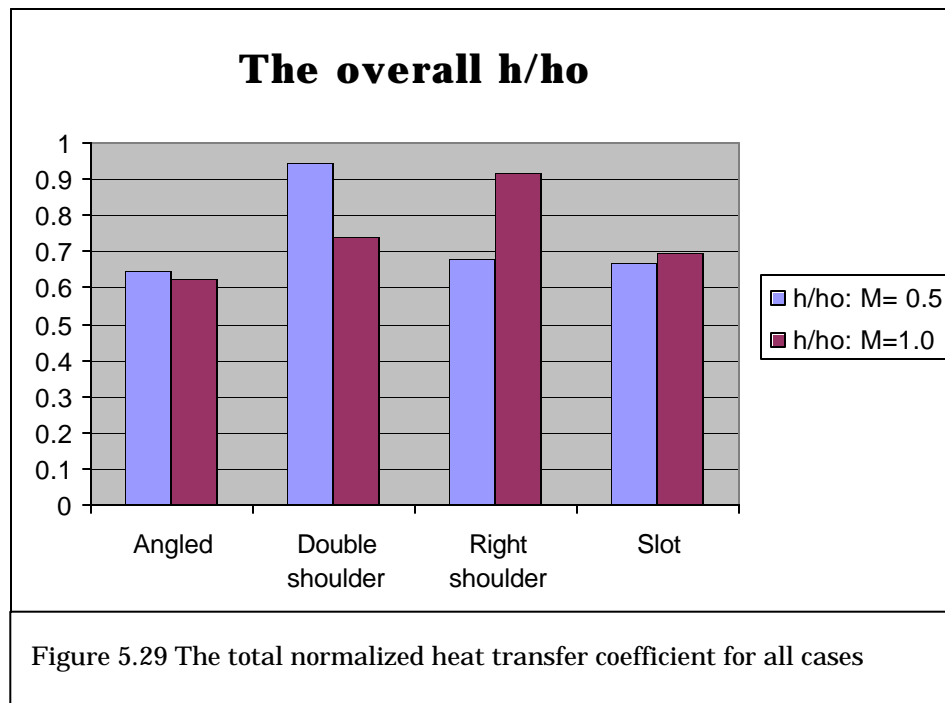


Figure 5.26 Normalized η for Angled case



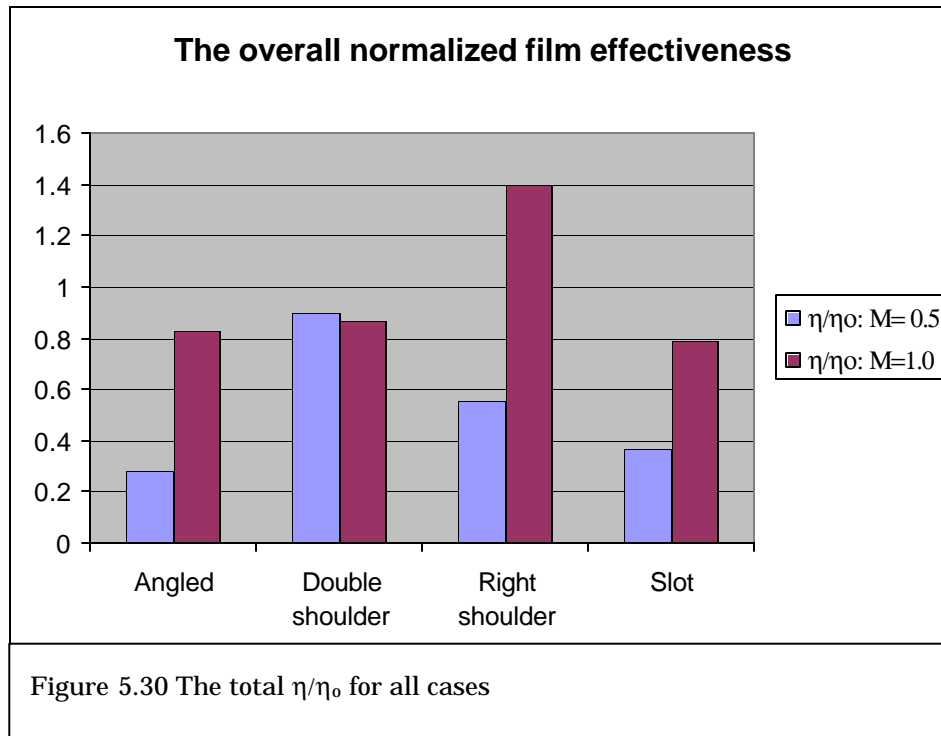
5.6 Summary of Cases:

The overall performance of all cases can be summarized in Figures 5.29 and 5.30. The first Figure shows the total normalized heat transfer coefficient for all cases. This is obtained by summing up all the span-averaged values for the entire X/d range. The second Figure was obtained using the same method but for the normalized film effectiveness factor.



Looking at both Figures shows that the slot and the angled are lowest in term of the total normalized heat transfer coefficient. This means both cases exchange less heat with the mainstream compared to the baseline case. However, the poor film effectiveness performance for both cases seen in Figure 5.30 rules them out as a better choice for cooling the blade. The remaining two cases are the double and right shoulder. The double shoulder showed good potential for exchanging less heat with the hot mainstream once its cooling jet mass flow was increased to meet $M=1.0$. even

its low blowing ratio was less than unity for the total h/h_o . The double shoulder could be a good option if its film effectiveness were above unity as its film effectiveness performed less than the baseline case. We also recall from the previous Figures that the double shoulder case did not have a stable film. As a result the double shoulder geometry may not be chosen a better cooling option.



The last case is the winning one. The right shoulder geometry held the highest adiabatic film effectiveness values among all tested geometries. That applies only to the high blowing ratio since the $M=0.5$ scored inadequately for the normalized η . In addition, the double shoulder geometry presented a unwavering film throughout the full range of tested plate. This case will provide a better cooling option than the baseline case and will supply a thicker film protecting blade from the hot flow.

Chapter 6

Conclusions

The intent of this study was to come up with an optimum hole exit geometry that can be incorporated in the new blade designs with lesser complications. This optimum geometry should not be associated with high convective heat transfer coefficient h . Also the adiabatic film effectiveness η should be as high as possible. For this purpose, different hole exit geometries were tested for an optimum shape. Heat transfer calculations were made to obtain the local values for h and η . The first cases tested were the “normal” 35° 0.5 inch diameter inclined hole. The first case tested were the “normal” 35° with 0.5 inch diameter inclined hole. The second was the “slot” with height to hole diameter ratio (p/d) is 0.4 and width to hole diameter ratio (W/d) = 1.75. The third was the right shoulder with (W/d) = 1.375. The fourth and fifth cases are the “double shoulder” with (W/d)= 1.0 and the “angled” with a varying ratio (W/d). The angled is featured with 18° inclined right attachment. The results of all cases were referenced to the normal case as a baseline.

The right shoulder case presented the best performance with a uniform jet spreading. The right shoulder geometry is more likely to protect and cool the blade than the normal geometry, as its total adiabatic film effectiveness was better than baseline case with factor of 1.4 and the total heat transfer coefficient was less than baseline case with factor of 0.08. This means the right shoulder geometry is more likely to protect and cool the blade than the normal geometry as it is going to exchange less heat and provide thicker film protection.

6.1 Recommendation for Future Work

The understanding of the film behavior requires more detailed measurements than heat transfer analysis. The deriving force for higher or lower h and \mathbf{h} depends highly on the flow pattern and local values for turbulence intensity. For this I recommend the following to be performed as future work for this study:

- (i) A detailed study on flow patterns where the turbulence intensity velocity values are measured locally. This should provide better insight of the two flow mixing behavior.
- (ii) Further heat transfer analysis investigation of higher blowing ratio for the right shoulder case. Suggested blowing ratios are 0.3 increments between 0.5 and 1.5

References

Ronald S. Bunker, 2002, "Film Cooling Effectiveness due to Discrete Holes Within transverse surface slot," *International Gas turbine and Aeroengine Congress & Exhibition*.

Ekkad, S. V., Zapata, D., and Han, J. C., 1997a, "Heat Transfer Coefficients Over a Flat Surface with Air and CO₂ Injection Through Compound Angle Holes Using a Transient Liquid Crystal Image Method," *ASME Journal of Turbomachinery*, Vol. 119, pp. 580-586.

Ekkad, S. V., Zapata, D., and Han, J.C., 1997b, "Film Effectiveness Over a Flat Surface with Air and CO₂ Injection Through Compound Angle Holes Using a Transient Liquid Crystal Image Method," *ASME Journal of Turbomachinery*, Vol. 119, pp. 587-593.

Eriksen, V. L., and Goldstein, R. J., 1974, "Heat Transfer and Film Cooling Following Injection Through Inclined Circular Holes," *ASME Journal of Heat Transfer*, Vol. 96, pp. 239-245.

Goldstein, R. J., Eckert, E. R. G., and Burgraff, F., 1974, "Effects of Hole Geometry and Density on Three-Dimensional Film Cooling," *International Journal of Heat and Mass Transfer*, Vol. 17, pp. 595-605.

Goldstein, R. J., and Taylor, J. R., 1982, "Mass Transfer in the Neighborhood of Jets Entering a Crossflow," *ASME Journal of Heat Transfer*, Vol. 104, pp. 715-721.

Gritsch, M., Schulz, A., and Wittig, S., 1998a, "Heat Transfer Coefficient Measurements of Film Cooling Holes with Expanded Slots," ASME Paper 98-GT-28.

Gritsch, M., Schulz, A., and Wittig, S., 1998b, "Adiabatic Wall Effectiveness Measurements of Film Cooling Holes with Expanded Exits," *ASME Journal of Turbomachinery*, Vol. 120, pp. 549-556.

Je-Chin Han, Sandip Dutta, Srinath Ekkad, 2000, "Gas Turbine Heat Transfer and Cooling Technology," New York : Taylor & Francis.

Hasan N., Acharya S., Ekkad S. V., 2001, "Film Cooling From a Single Row of Cylindrical Angled Holes With Triangular Tabs Having Different Orientation", *International Gas turbine and Aeroengine Congress & Exhibition*.

Hay, N., Lampard, D., and Saluja, C. L., 1985, "Effect of Cooling Films on the Heat Transfer Coefficient on a Flat Plate with Zero Mainstream Pressure Gradient," *ASME Journal of Engineering for Gas Turbines and Power*, Vol. 107, pp. 105-110.

Ligrani, P.M., Wigle, J.M., Ciriello, S., and Jackson, S.W., 1994a, "Film-Cooling From Holes with Compound Angle Orientations: Part 1-Results Downstream of Two Staggered Rows of Holes with 3d Spanwise Spacing," *ASME Journal of Heat Transfer*, Vol. 116, pp. 341-352.

Ligrani, P.M., Wigle, J.M., and Jackson, S.W., 1994b, "Film-Cooling From Holes with Compound Angle Orientations: Part 2-Results Downstream of a Single Row of Holes with 6d Spanwise Spacing," *ASME Journal of Heat Transfer*, Vol. 116, pp. 353-362.

Schmidt, D.L., Sen, B., and Bogard, D.G., 1996, "Film Cooling with Compound Angle Holes: Adiabatic Effectiveness," *ASME Journal of Turbomachinery*, Vol. 118, pp. 807-813.

Sen, B., Schmidt, D.L., and Bogard, D.G., 1996, "Film Cooling with Compound Angle Holes: Heat Transfer," *ASME Journal of Turbomachinery*, Vol. 118, pp. 801-807.

M. E. Taslim, 1992, "Experimental Investigation of Film Cooling Effectiveness for Slot of Various Exit Geometries," *Journal of Thermodynamics and Heat Transfer*, Vol. 6, No. 2,

Vita

Mohammed Altorairi was born on September 5th, 1972, in Alkhobar, Saudi Arabia. He received a degree of Bachelor of Science in Applied Mechanical Engineering from King Fahad University of Petroleum and Minerals (KFUPM), Dhahran, Saudi Arabia, in 1996. Mohammed worked for Saudi Aramco Oil Company as a “Custody Measurement Engineer” till he joined the Louisiana State University Mechanical Engineering graduate program in Fall 2001. He is a candidate for the degree of Master of Science in Mechanical Engineering for Summer 2003. Mohammed will return back to his work at Aramco in September 2003.